INVESTIGATION INTO THE EFFECT OF ROTATIONALLY SHIFTED ARCING HORNS ON A SUB-TRANSMISSION 132kV SYSTEM

BRETT SMITH

A dissertation submitted to the School of Engineering, University of KwaZulu-Natal, Durban, in fulfilment of the requirements for the degree of Master of Science

November 10, 2016

Supervisor: Dr. A.G. Swanson
Co- Supervisor: Dr. L. Jarvis

Declaration 1 - Plagiarism

I, Andrew Swanson, as the candidate's Supervisor agree to the submission of this thesis.

Acknowledged by Andrew Swanson on November 10, 2016
Signature:

I, Brett Smith, declare that

1. The research reported in this thesis, except where otherwise indicated, is my original research.

2. This thesis has not been submitted for any degree or examination at any other university.

3. This thesis does not contain other persons data, pictures, graphs or other information, unless specifically acknowledged as being sourced from other persons.

4. This thesis does not contain other persons' writing, unless specifically acknowledged as being sourced from other researchers. Where other written sources have been quoted, then:
a. Their words have been re-written but the general information attributed to them has been referenced
b. Where their exact words have been used, then their writing has been placed in italics and inside quotation marks, and referenced.

5. This thesis does not contain text, graphics or tables copied and pasted from the Internet, unless specifically acknowledged, and the source being detailed in the thesis and in the References sections.

Acknowledged by Brett Smith on November 10, 2016
Signature:

Declarations 2 - Publications

Details of contributions to publications that form part and/or include research presented in this thesis:

Paper 1: B.A.Smith, A.G Swanson, "Investigation into the role of arcing horns on 132kV sub-transmission infrastructure.", Southern African Universities Power Engineering Conference, 2016

Paper 2: B.A.Smith, A.G Swanson, "Validation of the breakdown mechanism between rotated arcing horns." , Southern African Universities Power Engineering Conference, 2016

Acknowledgements

I would like to thank my supervisor Dr Andrew Swanson for all his support, motivation and guidance throughout my Masters research. I feel I have benefited from your mentorship and professionalism and endeavour to continue with knowledge expansion into the field of High Voltage engineering.

EPPEI CoE must be acknowledged for providing me with a platform from which to present and collaborate my research. Through the CoE I was privileged enough to attend the Southern Africa Universities Conference(SAUPEC) to present my findings in the plenary session.

The University of KwaZulu-Natal needs to be acknowledged for allowing the use of the High Voltage Laboratory in which to perform my experimental work. Thanks go to the workshop staff who were always on hand to assist me.

eThekwini Municipality for providing me with insulators and arcing horns for the purposes of conducting my experiments in the laboratory. In particular, Mr Raj Dhrochand for providing me with the original idea for the formulation of this dissertation.

Last, but not least, I would like to thank my family, my friends and my girlfriend for their endless support during my research.

Abstract

Insulators perform a vital role in a high voltage transmission system as they are expected to withstand normal operating voltages as well as external overvoltages such as those caused by lightning strikes.

These arcing horns are primarily fitted to protect the insulator against arc damage in the event of a flashover occurring. In addition to this, they perform a role in the insulation level of the sub-transmission system by providing coordinated protection from backflashover events that are caused by direct strikes to transmission towers.

Currently, the eThekwini Municipality maintains the need of placing arcing horns on their 132kV insulators within a certain span length of a nearby substation. The arcing horns are subject to rotational shifts in the event of adverse weather conditions and this leads to unscheduled maintenance and replacement of the insulator arcing horn arrangement. This upkeep is both costly and time consuming and is a process which may not be necessary. The rotational shift leads to a longer flashover distance and higher breakdown strength and implies that the system will be better protected against flashover and backflashover. However the integrity of the insulation co-ordination of the system is compromised in the process.

This work investigates the effect of the rotation of the arcing horns on both the protection of the insulator as well as the sub-transmission system by means of an insulation co-ordination study implemented in ATP/EMTP. The study was used to determine the probability of a lightning strike causing backflashover.

The model in ATP/EMTP was dependent on a leader progression model and an experiment, conducted on 22kV and 88kV insulators, to validate the breakdown mechanism was undertaken. It was noted that different breakdown mechanisms exist for varying spark gap distances which could influence the trend of the results; a correlation between the model and the experiment was derived.

The rotation of arcing horns on the insulators do not require immediate maintenance or replacement of the unit. The leader progression model yielded results in conjunction with the experiment which indicate the lowest possible breakdown voltages for each rotated arrangement. While allowing the arcing horns to rotate result in greater system protection by increasing the basic insulation level of the sub-transmission system and thereby decreases the occurrence of backflashover and the associated earth fault. The degree through which they rotate should be monitored as they could potentially pose an issue to the insulation co-ordination of the system.

Contents

List of Figures

List of Tables

List of Symbols

Chapter 2:

- E_{field} - Electric field strength
- n_t - Total amount of electrons
- n_c - Electrons emitted by the cathode
- α - First ionisation co-efficient
- n_0 - Electrons initially present at cathode
- d - Distance between anode and cathode
- γ - Secondary ionisation co-efficient
- η - Attachment co-efficient
- i_0 - Saturation current
- V_{50} - Voltage which results in a 50% probability of breakdown
- σ - Standard deviation
- μs - Microsecond
- I_c - Mean lightning current amplitude
- U_m Peak voltage
- t_f - Value used to calculate τ_1
- t_h - Value used to calculate τ_2
- h - Height of tower

- b - Overhead ground wire separation

Chapter 3:

- U_{50} - Experimental value of V_{50}
- V-t - Volt-time
- L - Length of gap for V-t curve
- t_b - Total time to breakdown
- t_i - Time to corona inception
- t_s - Time for streamer development
- t_l - Leader formation
- E_{max} - Maximum electric field found in a spark gap
- E_{50} - Critical electric field breakdown for a rod-rod gap
- k - Gap factor
- $\frac{dl}{dt}$ - Velocity of leader
- d_i - Spark gap distance for gaps less than 1 meter
- V_{sp} - Flashover voltage for gaps less than 1 meter
- x - Initial spark gap distance of separated arcing horns
- r - radial height of arcing horn above insulator
- θ - Horizontal rotation degree of arcing horns
- d_{gap} Distance between rotated arcing horns
- k - Humidity correction factor
- σ - Temperature correction factor
- b_0 - Standard atmospheric pressure
- t_0 - Standard room temperature
- N - Number of impulses applied to test arrangement

- $s_{measure}$ - Scaling ratio of impulse measurement circuit
- d_{ratio} - Ratio of capacitive divider

Chapter 4:

- Z_T - Surge impedance of tower
- Z_g - Surge impedance of ground wire
- I_{stroke} - Amplitude of lightning stroke
- V_{top} - Voltage at the top of the tower
- h_k - Effective height of tower section
- r_{ak} - Effective radius of the cross arm
- Z_1, Z_2 - Surge impedances at a boundary
- ρ_{12} - Reflection co-efficient at a boundary
- $t_{10\%}$ - Time taken to reach 10% of peak value
- $t_{90\%}$ - Time taken to reach 90% of peak value

Nomenclature

- CFO - Critical flash over
- ATP - Alternative transients programme
- EMTP - Electromagnetic transients programme
- IEC - International Electrotechnical Commission
- CD - Creepage distance
- SCD - Specific creepage distance
- USCD - Unified specific creepage distance
- BIL - Basic insulation level
- BSL - Basic switching level
- OHGW - Overhead ground wire
- TD - Thunderstorm days
- DUT - Device under test
- DE - Disruptive effect
- LPM - Leader progression model
- TLSA -Transmission line surge arrester
- BFO - Backflashover
- CT - Current transformer
- CB - Circuit breaker

- AC - Apparatus connection
- IEEE- Institute of Electrical and Electronic Engineers
- WG - Work group
- TRV - Transient recovery voltage

Chapter 1

Introduction

Power systems are exposed to regular overvoltages including temporary overvoltages, related to power frequency or system harmonics, and transient overvoltages that can be generated internally as a result of connecting or disconnecting the system; or externally, due to atmospheric phenomena such as lightning [1]. While the effects of an internal overvoltage are proportional to the operating voltage of the system; the magnitude of an external overvoltage is independent of the system voltage.

This study deals with a 132kV sub-transmission system. This system should be primarily designed to withstand lightning overvoltages [1]. The distribution system of Durban (eThekweni) Municipality is to be studied and this distribution scheme specifically makes use of polymeric insulators fitted with arcing horns on the live side of the insulator or on either side within close proximity of their substations. As far as the author is aware, this practice is not used elsewhere in this configuration.

Arcing horns are projecting conductors used to protect insulators from flashover damage to the insulator and end fittings by providing a suitable path for discharge between them; they are mechanically attached to the end fittings of insulators and have varying shapes and orientations. These arcing horns could, additionally, be seen as part of insulation co-ordination as they can be configured to protect the substation from high lightning currents by setting the distance between the arcing horns to flashover at a certain critical flashover (CFO) voltage.

Adverse weather conditions such as those experienced in a strong storm can cause these arcing horns to shift away from their original position. This shift can be problematic as it can alter the CFO voltage of the transmission system and cause the arcing horn spark gap to maloperate.

Maintenance and inspection of these insulators and arcing horns is an important aspect in the lifespan of any electrical network. Presently, it has not been decided as to how severely shifted the arcing horns need to be to warrant maintenance. This practise is both time-consuming and costly as it may require the line to be de-energised.

It is therefore necessary to investigate aspects relating to the breakdown of the arcing horn spark gap after it has undergone a rotational shift. It is also necessary to undertake an insulation co-ordination study as the protection of the system can also be influenced by the movement of these arcing horns in conjunction with other aspects such as earth resistance.

1.1 Research questions

The research questions to be answered include:

- How will the the breakdown voltage of the sparkgap change due to a rotational shift of one arcing horn relative to the other and furthermore, at which point in the rotation is the CFO voltage of the spark gap large enough to require maintenance to prevent disruption to the insulation co-ordination?
- Is the practice of having two arcing horns fitted on an insulator within 1.5 km of a substation not necessary when used in conjunction with nearby surge arresters?
- How will the breakdown mechanism be affected when the arcing horns are rotated through an angle relative to one another?

1.2 Hypotheses

The hypotheses for this dissertation are as follows:

- A shift in the arcing horn arrangement does not require immediate maintenance. The breakdown voltage will increase as the spacing between the arcing horns increases. If the CFO voltage of the gap poses a threat to insulation co-ordination then that gap distance and rotation must be noted as being large enough to require maintenance.
- Surge arresters form part of the system's insulation co-ordination. Having arcing horns fitted on both ends of the insulator may help in the protection of the insulator surface in the event of flashover and therefore should be able to be used in conjunction with a surge arrester.
- The breakdown mechanism between the arcing horns may change as the rotation increases. Flashover to the end fitting of the insulator may take place at higher degrees of rotation.

1.3 Importance of research

This research endeavours to quantify the non-replacement of the insulator-arcing horn unit should a shift occur and attempts to propose the positive aspects which may be provided to a system in this case.

1.4 Scope and dissertation layout

The scope of this dissertation includes the modelling of all aspects of the insulation co-ordination study including components such as the metal oxide surge arrester, the transformer, transmission lines and the surge impedance model of each transmission tower.

The insulation co-ordination model utilises an earth resistance to conduct a sensitivity study to estimate the voltages across the spark gap created by the rotation of arcing horns under extreme weather conditions when a lightning impulse is imposed on a transmission tower structure. The purpose of the study is to best estimate the probability relating the lightning amplitude of

the strike to the degree of rotation of the arcing horn and that of the earth resistance.

A laboratory experiment was conducted to attempt to confirm the breakdown mechanism of the spark gap in the case of each point of rotation. The experiment was conducted for both polarities of impulse and the results were related back to theoretical values.

Chapter 2 takes a closer look at insulators and insulation co-ordination and the related aspects surrounding them.

The laboratory work conducted on the 22kV and 88kV insulators is introduced in Chapter 3. A comparison between theoretical and practical results is illustrated.

Chapter 4 deals with the insulation co-ordination, the sensitivity study and the modelling of the sub-transmission system in ATP-EMTP.

The conclusions and findings of the research are presented in Chapter 5 along with potential considerations and suggestions which could relate to similar future work.

Chapter 2

Insulators and Insulation Co-ordination

Insulators are used to prevent currents from high voltage sources from reaching earth. In the case of an overhead line, the insulation consists of non conductive material to mechanically and electrically separate the live conductor from the tower by means of an air gap.

Insulators are not perfect in nature as they are unable to protect against all instances of overvoltages. This is due to their design being limited by economic viability. Insulation co-ordination is therefore required. This process, or technique, is used to provide controlled risk to equipment.

Figure 2.1 illustrates clearly the type of insulation set up that will be dealt with. In the Figure the high voltage line entering from the left hand side is separated from the tower, or earth, on the right by a polymeric insulator. The insulator is fitted with an arcing horn arrangement. The importance of these arcing horn structures will be discussed in Section 2.4

This chapter introduces aspects of the insulation including line insulators and breakdown in air as well as the insulation co-ordination that will be assessed in the study.

Figure 2.1: Arcing horn arrangement on a 132kV transmission line near substation

2.1 Insulators

Insulators consist of an insulating body, made of either porcelain, toughened glass or a fibre-reinforced plastic. Insulators can be classified into two broad categories namely ceramic and non-ceramic. Ceramic insulators are characterised by glass and porcelain while polymer insulators are classified as non-ceramic [1]. More specifically insulators may be classified by the materials from which they are made; and can thus be divided into three main categories.

- Glass
- Porcelain
- Polymer

Since eThekwini Municipality uses polymer insulators on their transmission lines glass and porcelain insulators will be considered as outside the scope of this study.

2.1.1 Insulator characteristics

In order to successfully classify insulators parameters to their relative performance some general parameters have been devised [6].

- **Section Length.** The section length refers to the shortest distance between the fixed connection points of the live and earth metal joints. The section length can be observed in Figure 2.2.
- **Dry arc distance.** This is the shortest distance in the air external to the insulator itself that will maintain the operating voltage. In the case of an insulator equipped with arcing horns as seen in Figure 2.2; the arcing horns will govern the dry arc distance; this is important when considering rotation.
- **Strike distance.** The shortest distance from the high voltage side of the insulator to the ground side. Depending on insulator contamination this distance may correspond to the dry arc distance.
- **Creepage distance (CD) or leakage path.** The leakage distance is the shortest path across the insulator surface that could become conductive in case of pollution contamination. There is a directly proportional relationship between insulation strength and creepage distance. Pollution or contamination of the insulator string falls outside the scope of this dissertation and will not be discussed.
- **Specific Creepage Distance(SCD)** The specific creepage distance is defined as the total creepage path length divided by the phase-to-phase voltage of the maximum voltage which is experienced by the insulator. The common unit is expressed in mm/kV.

$$SCD = \frac{CD}{V_{pp}} \quad mm/kV \tag{2.1}$$

- **Unified Specific Creepage Distance (USCD)** The unified specific creepage distance (USCD) is defined as the specific creepage (SCD) multiplied by $\sqrt{3}$.

$$USCD = \sqrt{3} \times SCD \quad mm/kV \tag{2.2}$$

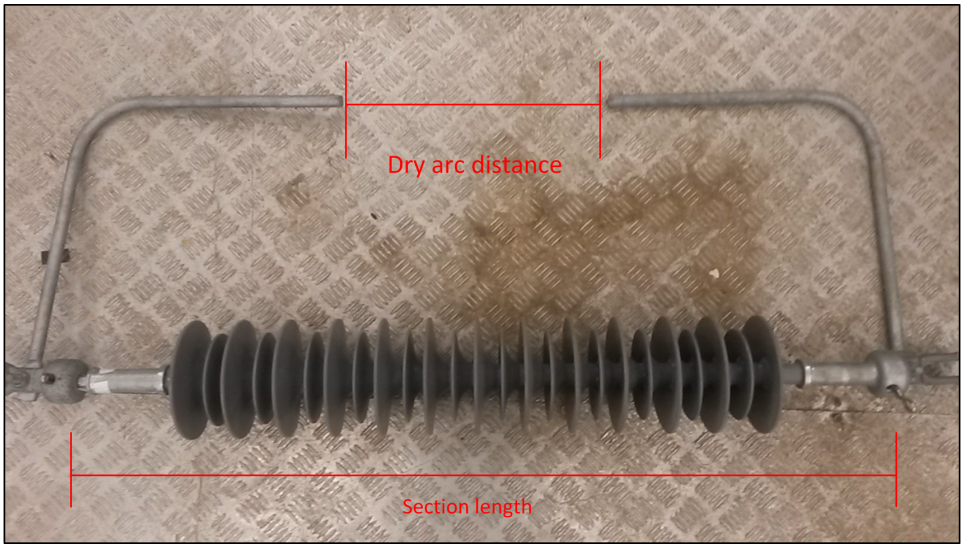

Figure 2.2: 88kV insulator test setup illustrating insulator characteristics

2.2 Breakdown

Breakdown which takes place across an insulator occurs in the presence of a sufficiently high electric field which is brought about by an overvoltage. The process can be described succinctly by splitting up the factors leading to eventual breakdown namely; the (i) the avalanche, (ii) the streamer and (iii) the leader formation.

2.2.1 Electron avalanche

Consider an electrode system where a high voltage, V measured in kV is applied between a gap of distance, d creating an electric field, E_0 as seen in equation (2.3)

$$E_0 = \frac{V}{d} \quad kV/m \tag{2.3}$$

As the voltage, V_1 is applied the free electrons, which may be produced near the positively charge cathode by a natural ionisation process or be illuminated by ultraviolet light, are accelerated into the gap by the electric field toward the anode creating an initial current i_0. Figure 2.3 refers.

Townsend introduced a quantity known as α or **Townsend's first ionisation co-efficient** to describe the exponential current increase after voltage

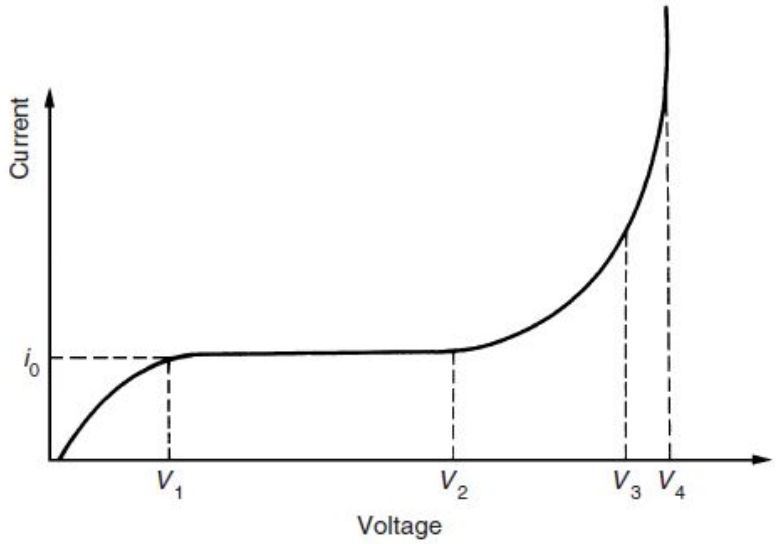

Figure 2.3: Voltage current relationship - as seen in [1]

V_2 stating that once electrons are accelerated sufficiently they are able to cause ionisation on impact. An equation governing the amount of electrons over the distance d, can be then be given by equation (2.4)

$$n_c = n_0 e^{\alpha d} \tag{2.4}$$

where n_0 is the initial amount of electrons found at the cathode and n_c is the total amount of electrons produced by other electrons in the direction of the electric field. The exponential term, $e^{\alpha d}$ is called the electron avalanche and governs the number of electrons a moving electron will create moving across the electric field. It must be noted however, that in an air gap electronegative gas components such as oxygen and nitrogen some of the electrons attach themselves to these neutral molecules to become negative ions yielding an ***attachment co-efficient***, η, and thus the effective ionisation co-efficient becomes $(\alpha - \eta)$. Thus, the new expression becomes

$$n_c = n_0 e^{(\alpha - \eta)d} \tag{2.5}$$

The exponential rise in current can be found in equation (2.6)

$$i = i_0 e^{(\alpha-\eta)d} \tag{2.6}$$

2.2.2 Streamer development

The $e^{\alpha d}$ term is only valid so long as the space charge created by the electrons and ions can be neglected compared to the originally applied electric field, E_0 [1]. When the concentration of the electrons exceed 10^8 the current rises exponentially as a result of a distortion of the original field by the space charge created by the electron avalanche. This can be represented by equation (2.7) and Figure 2.4.

$$n_c = n_0 e^{(\alpha-\eta)d} = 10^8 \tag{2.7}$$

The condition that the field created by the space charge assumes a similar value to that of the external field creates the first criterion required for an avalanche to transition into a streamer. Once the avalanche has crossed the gap, d, the streamer mechanism will breakdown the gap.
The development of streamers are generally found in smaller, shorter gaps. In the case of larger gaps, streamers are usually accompanied by the formation of leaders.

2.2.3 Leader development

Corona is a bluish discharge formed when the air is ionised. Although not always directly accompanied by flashover the mechanics of the formation of corona is useful to consider when dealing with breakdown in uniform or non-uniform electric fields.
In the first stage there is ***no discharge*** present while the voltage rises from zero to the corona inception voltage. A certain level of voltage will result in the first appearance of corona otherwise known as ***first corona***. Corona appears as a collection of small streamers that originate from the high-voltage electrode. The streamers appear as a slight hue of blue light and each one follows a different path from the previous, however, there does exist one stem which is common to all. Streamers have the ability to travel at a velocity of a few meters per microsecond and for divergent field distributions have the ability to span gaps up to distances of a few tens of centimetres up to a few metres.

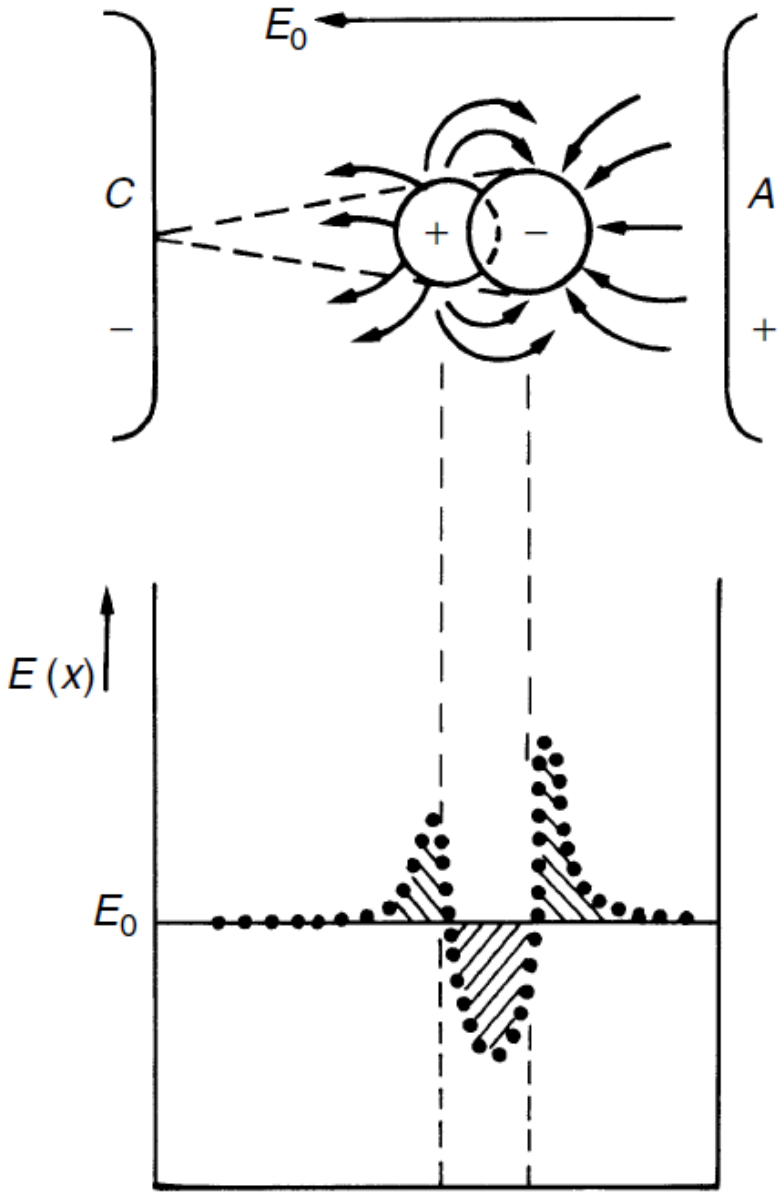

Figure 2.4: Uniform field distortion caused by space charge - as seen in [1]

First corona may be followed by a ***dark period*** during which there exists no discharge activity as the space charge produced by the streamers reduces the electric field at the electrode below the critical corona inception voltage. Following the dark period, a second burst of corona can occur depending on the non-uniformity of the electric field [7]. Should the field be uniform, the streamers will reach the ground electrode leading to an increase in discharge current until breakdown occurs.

The most pivotal moment in any flashover process is the ***formation of a leader*** and the propagation of that leader in a gap. Regardless of whether a dark period exists within the process; corona is followed by a highly ionised channel termed a leader. The leader originates from the tip of the streamer stem and possesses a large magnitude of the electric field at its tip resulting in leader corona formation.

The final stage of flashover occurs when the leader has bridged about two-thirds of the gap and the ***final jump*** occurs. The leader velocity increases dramatically and "jumps" to its final destination. The final jump is said to have occurred when the streamers from the tip of the grounded electrode meet those from the high voltage electrode.

No significant discharge activity is usually found at the grounded or negative electrode until the process is almost at its conclusion.

It should be noted that leader initiation and propagation depend both on the geometry of the electrodes as well as the crest and shape of the applied voltage waveform. There are critical waveforms which can cause flashover with the lowest possible crest value; these waveforms have been determined experimentally for a number of gaps. Previous flashover models have sought to predict the critical flashover voltage for a specified gap under external conditions using a leader progression model (LPM) as seen in [8, 9].

2.3 The statistical nature of the breakdown process

The statistical nature of breakdown in a gaseous dielectric is rather apparent in impulse breakdown and self restoring insulation materials such as air [10]. The statistical nature can be attributed to the high variability of the position electrons at an atomic level. Additionally, a formative time lag exists which takes into account the time needed for the development of the avalanche and as a result gives rise to a statistical fluctuation of the time to breakdown of an insulation element; seemingly in the same conditions. The different times involved in the breakdown process are discussed in Section 3.2.3. As such, the flashover voltage may only be expressed in terms of a probability. The V_{50}, or CFO voltage, is the voltage at which 50% of the applied impulses result in a flashover. The flashover probability does differ with voltage according to a Gaussian distribution. The equation for flashover vs. voltage is represented by the following expression:

$$p(V) = \frac{1}{\sigma\sqrt{2\pi}} \int_{-\infty}^{V} e^{-\frac{1}{2}(\frac{x-V_{50}}{\sigma})^2} dx \tag{2.8}$$

where p(V) is the flashover probability, V_{50} is the voltage corresponding to a 50% probability of flashover and σ is the standard deviation.

The basic insulation level (BIL) of a system can be related to the CFO voltage in that the BIL voltage level should have a 10% probability of experiencing flashover. Thus, if a standard deviation of Gaussian distribution can be defined as σ_f then the BIL found within 1.28 standard deviations of the CFO as stated in [10] and can be related to the CFO voltage by the following equation.

$$BIL = CFO(1 - 1.28\frac{\sigma_f}{CFO}) \tag{2.9}$$

The equation applies to both lightning (BIL) and basic switching levels (BSL) although the value of sigma can range between 2-3% for lightning and 5-7% for switching impulses. The conventional form of BIL applies to non-self restoring insulation and does not possess a value for CFO voltage. This is due to the BIL value being defined as the voltage value equal to that

of the point of flashover.

2.4 Electric Field on insulators and grading rings

The electric field distribution on the surface of a polymeric insulator installed on a transmission line is a function of numerous parameters including the voltage class, insulator design, tower configuration and phase spacing.

Generally, the electric field magnitudes are far larger toward the energised fitting of an insulator where, in some cases, the highest field potential is adjacent to the end fitting.

2.4.1 Factors influencing electric field distribution

There are a number of factors that influence polymeric insulator field distribution. The most important ones include [11].

1. Insulator geometry which includes the weathershed, fibreglass rod and the end fittings.
2. Electrical properties of the polymer material and any semi-conductive material that may be present.
3. The dimensions and position of corona rings, as well as attachment hardware.
4. The geometry of the attachment hardware such as arcing horns.
5. The orientation of the attachment hardware and its physical relationship to the attachment hardware.
6. The energised line voltage.
7. Presence and interference of nearby phases.

Each of these parameters should be taken into account when determining the electric field distribution of a polymer insulator utilising either modelling or measurement.

The dependence of the electric field distributions on these parameters means that identical insulators applied in many various orientations will yield different field distributions; and therefore different breakdown behaviour. The flashover, or backflashover behaviour of the system could be directly influenced by these external factors. Application of this topic can be found in Chapters 3 and 4.

2.4.2 Regions of interest

There are three main regions of interest when it comes to analysis of electric field distribution.

1. Inside the fibreglass rod and watershed material.
2. On the surface, and in the air surrounding, the insulator surface as well as the end fitting seals.
3. On and in the air surrounding metallic end fitting such as corona rings or arcing horns.

Should the field distribution in any of these regions exceed critical values, unwanted or excessively large magnitudes of discharge activity may occur which could affect both short and long term performance of the insulator. Points 2 and 3 are relevant to this study as the arcing horns are attached as the end fittings on both sides of the insulator. Figure 2.5 refers.

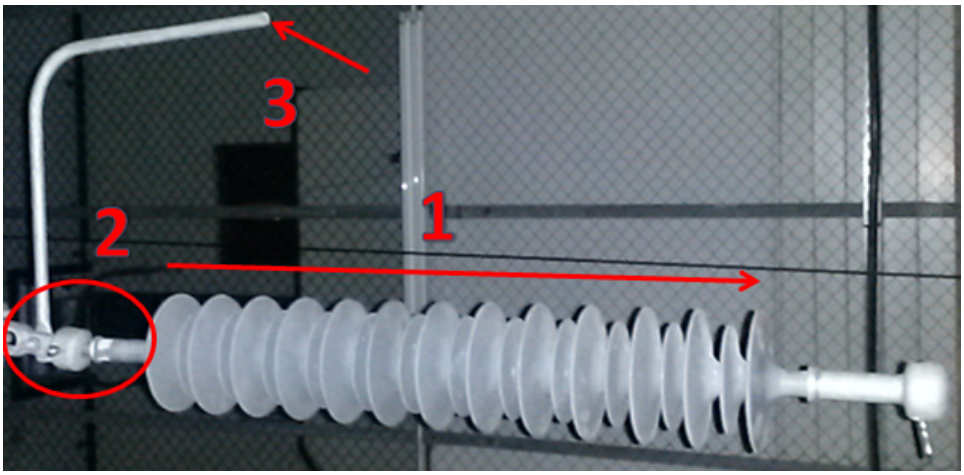

Figure 2.5: 88kV insulator with regions highlighted

2.4.3 Control of the electric field distribution

The electric field distribution may be controlled by the following mechanisms as mentioned in [11].

1. **Polymer end fitting design.** The design has an influence on electric field distribution within the polymer insulator as well as on the surface of the weathershed material. Large end fittings with rounded edges tend to reduce the maximum field magnitude. This grading of the field is integral in the design of the insulator.

2. **Corona ring application and design.** Appropriately designed corona rings are also utilised to reduce steep field gradients while moving the large magnitudes of the field away from the end fitting. The positioning of the grading or corona rings may have a significant impact on the field distribution.

Figure 2.6: Corona rings used to control electric field distribution

3. **Application and Design of Extra Hardware.** The application of extra hardware, such as arcing horns or additional grading devices,

influence the field distribution of the polymer insulator. For example, if an arcing horn is applied, the maximum electric field may be reduced. Any hardware that is in close proximity to the insulator most impacts on the electric field distribution.

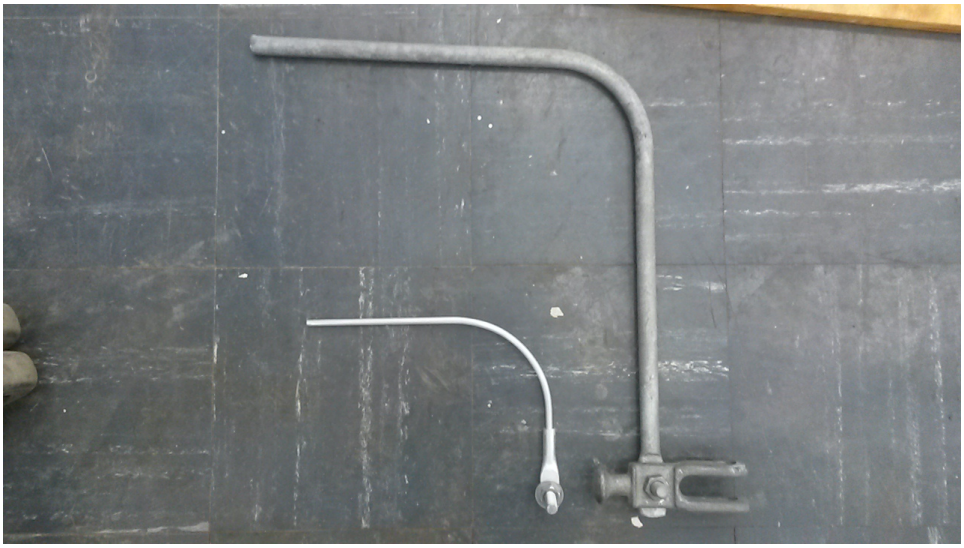

Figure 2.7: Various sized arcing horns

2.5 Insulator damage

Figure 2.8 and 2.9 illustrate the effect a flashover occurrence can have on an insulator in the situation where a relay senses an overvoltage and applies a trip signal to the circuit breaker. In the Figures a burn mark may be observed on both end fittings, while in Figure 2.9 the insulator sheath has also been damaged.

Figures 2.10 and 2.11 are examples of arc damage. When not extinguished by the system, arc damage can cause irreparable damage to the insulator unit. As a result it is imperative that arcing horns be utilised in order to protect the insulator against potential arc damage resulting from flashover.

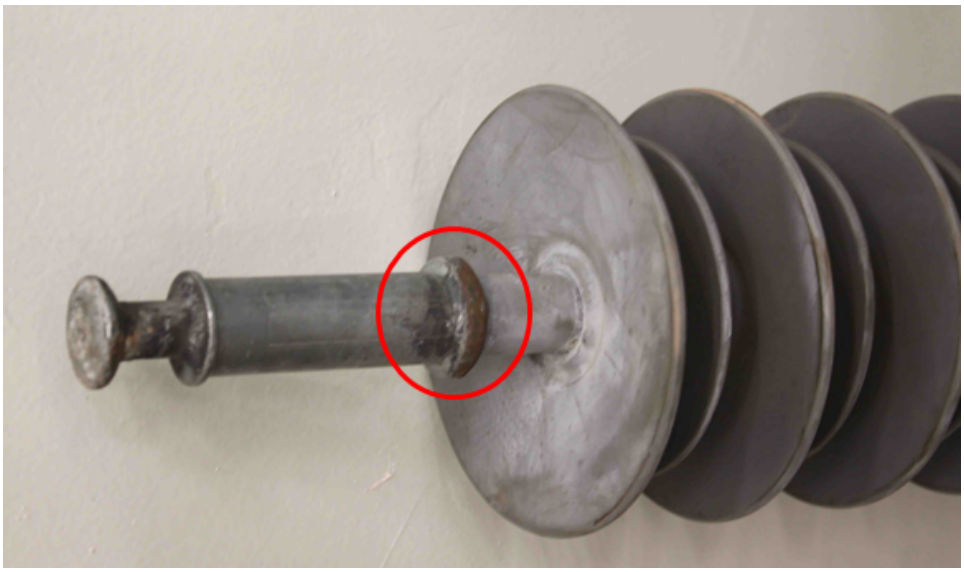

Figure 2.8: Burnt insulator fitting

Figure 2.9: Burnt insulator fitting with sheath damage

Figure 2.10: Severed end fitting as a result of arcing damage

Figure 2.11: Severely damaged insulator sheath

2.6 Insulation co-ordination

Insulation co-ordination is a technique utilised to ensure that various electrical items found in a distribution or transmission system are matched to system characteristics according to expected overvoltages and fall within expected voltage risk margins expressed through the use of voltage-time curves. Objectives which arise from analysis of co-ordination studies provide a means to assist in the reduction of system failures, while proportionately lessening the amount of supply interruptions caused by insulation breakdown to an acceptable level. According to [10] by selecting the minimum insulation strength, or minimum clearance, the minimum cost of the insulation can be attained.

The International Electrotechnical Commission (IEC) standard 60071.1 [12] which covers the topic of insulation co-ordination recognises that insulation may occasionally undergo failure as it is not economically feasible to eliminate failure completely.

2.6.1 System voltages

In order to succinctly introduce the topic of insulation co-ordination, a number of different aspects regarding the voltages and overvoltages should be covered. The characteristics of relevant insulation are also important in the fundamentals. Insulation levels within a system are always monitored and dependent on the highest system operating voltage and not on the nominal line voltage and therefore, in a 132kV system, the highest voltage is defined as 145kV [13].

Table 2.1: System voltages for a 132kV system- as seen in [1]

Nominal Voltage	132kV
Maximum Voltage	145kV
Power Frequency Withstand Voltage	230/275kV
Lightning Impulse Withstand Voltage	550/650kV
Switching Impulse Withstand Voltage	n/a

2.6.2 Temporary and switching overvoltages

Overvoltages can be electrical power generated within the system by the connection or disconnection of circuit elements [14]. Surges generated within the system can be further classified into two groups namely; *temporary overvoltages* in the case where they are of power frequency and weakly damped or *switching overvoltages* when highly damped and of short duration. A typical switching form is the 250/2500 μs, time-to-crest/time-to-half value wave. Switching impulses become relevant above voltage levels of 300kV [14]; due to the generated switching surges being directly related to the systems operating voltage. Diesendorf [14] states that the primary concerns for switching overvoltages include:

- Phase-to-earth faults
- Load rejection

Overvoltages involving both resonance and arcing ground faults are usually extinguished by system design and neutral earthing. Below distribution levels of 145kV, the method of earthing will determine the temporary level of overvoltage.

Insulation installed within a system should also be able to withstand short-duration power frequency overvoltages or for that matter, any other oscillatory voltages which possess the ability to last in the region of tens of seconds.

2.6.3 Lightning overvoltages

On power systems operating at 300kV and below, overvoltages occurring as a result of lightning will be of larger occurrence than those generated by internal phenomena. External overvoltages arise from lightning discharges and are characterised by the short duration 1.2/50 μs front time/time-to-half impulse waveform. Insulation flashover in the system can depend on a number of variables as mentioned in [15].

- The geographical position of the stroke
- The magnitude of the stroke

- The rise time of the stroke
- The insulation levels
- The local atmosphere or ambient conditions
- The system's electrical characteristics

The damaging return stroke of a lightning flash varies between 2kA- 200kA in accordance with a logarithmic-normal distribution [15]. Impulse rise times are in the order of tenths of microseconds for a negative flow of charge from cloud to ground while a positive flow can take considerably longer. The most severe lightning current of 200kA and rise time of 200kA/μs may be considered, if necessary, for design purposes. The mean probability of the current amplitude can be defined as I_c and can be found at $I_c = 31$kA

$$p(I > I_c) = \frac{1}{1 + (\frac{I}{I_c})^{2.6}} \tag{2.10}$$

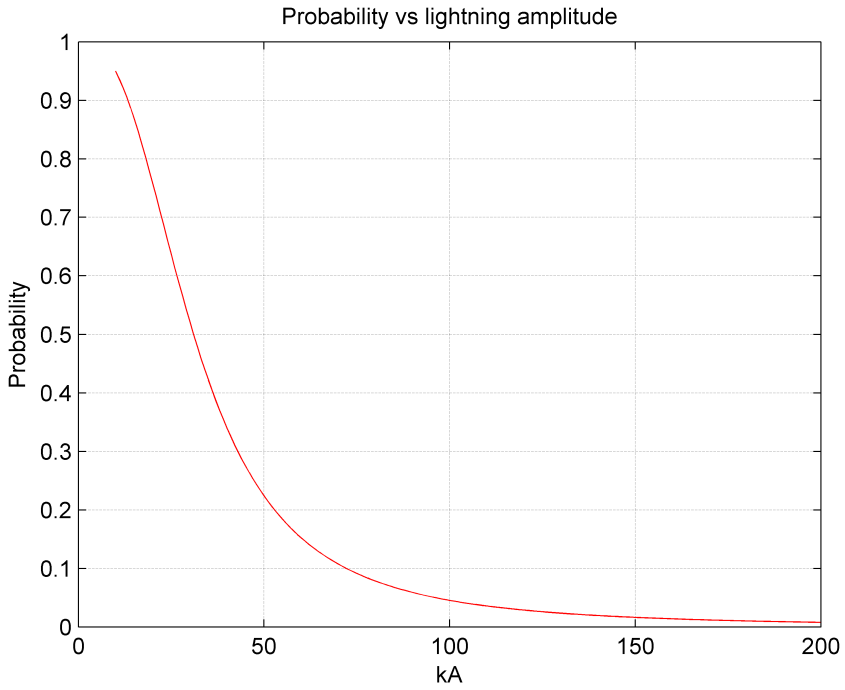

Figure 2.12: Probability distribution vs. lightning amplitude

2.7 Lightning

In order to describe the effect of lightning phenomena on transmission systems a few terms have been defined: [15]

- ***Flash***- a term which encompasses the entire discharge from the origin of the cloud to the struck object.
- ***Stroke***- The components within a flash which carry the high current components. A flash may contain one or more subsequent strokes.
- ***Flashover***- a discharge completed from an energised conductor to a grounded support.
- ***Backflashover***- a discharge completed from a earthed support to an energised conductor. This aspect is discussed in Chapter 4.
- ***Tripout***- a flashover or backflashover which does not extinguish itself. A circuit breaker must remove the ac power long enough to extinguish the arc.

There are many instances where lightning occurs over the design life of a transmission line. The initiation of a flashover, as a result of a lightning strike to a tower or shielding wire may result in a severe flash and detrimental damage to insulation.

2.7.1 Formation of the surge voltage waveshape

Lightning currents that are dealt with within the investigation, are required to be modelled within existing standards. Overvoltages corresponding to lightning impulses are unipolar in nature and may be represented by a waveform shown the Figure below.

The shape of the impulse consists of a fast-rising front followed by a slowly decaying tail after reaching the peak. The wavefront is usually characterised in terms of a peak value U_m, an equivalent front time t_f extrapolated from the 10% value to the 90% value, the time for the wave to decay its half value from the peak is termed t_h. The peak values of the impulse waveform are far higher than the corona onset voltage V_0 of the conductor or the conductor bundle on the transmission line.

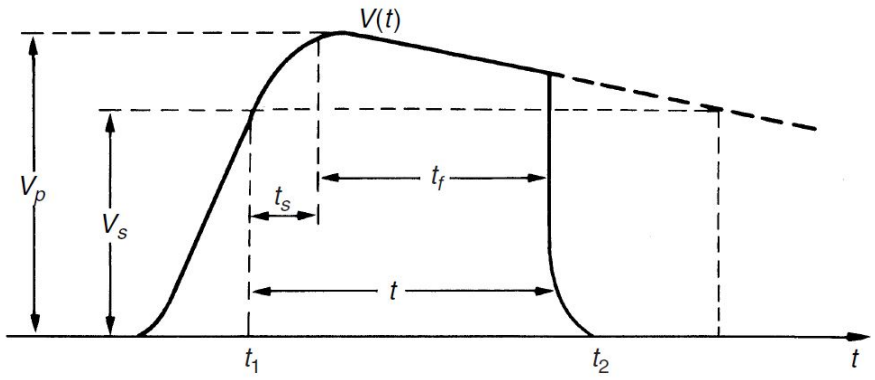

Figure 2.13: Impulse waveform - taken from [1]

Impulse voltages are usually specified in terms of their peak voltage U_m and the t_f/t_h values. The standard lightning impulse is specified in [16] as 1.2/50 μs as being the closest to a lightning waveshape. Currents measured through surge arresters also have longer front times of 4 to 8 μs when a 1.2/50 μs is applied which has subsequently led to the definition of the 4/10 μs and 8/20 μs current waveforms for testing purposes. It must be noted however; that these waveforms do not correspond well to the original parameters and should not be used for calculating lightning performance in the absence of surge arresters. IEC 60060-1 uses the double exponential expression to represent impulse waveforms.

$$I = I_{pk} \times K \times (e^{-t/\tau_1} - e^{-t/\tau_2}) \tag{2.11}$$

For a 1.2/50 μs wave the parameters are set as follows K = 1.037, t_f = 68.5 μs, t_h = 0.404 μs [15] where t_f is used as the value for τ_1, t_h is used to calculate τ_2 and K is a constant factor.

2.7.2 Ground flash density

The GFD in an area can be related to the number of thunderstorm days (TD) as defined by World Meteorological Association standards. GFD is usually expressed in flashes per square km per year. Generally, ten years of observations are needed in areas of moderate thunderstorm activity (40

days/year) to obtain a relative 5% standard deviation. The following expression for relating thunderstorm day levels in South Africa to ground flash density can be found in [10] as well as other references.

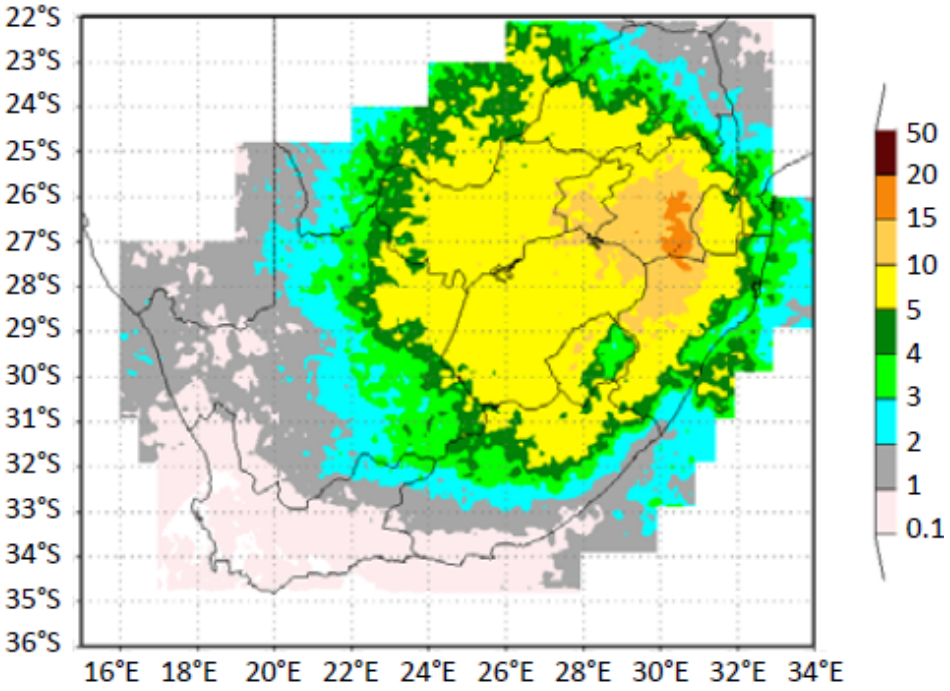

Figure 2.14: Cloud to ground flash density per kilometre in South Africa 2006-2010 [2]

$$GFD = 0.04 \times TD^{1.25} \tag{2.12}$$

The flash collection rate N_s represents the number of flashes over 100km per year. The expression for N_s depends on the GFD, the height of the tower and the overhead ground wire (OHGW) separation distance.

$$N_s = N_g \times \frac{28h^{0.6} + b}{10} \tag{2.13}$$

Where:
h = the height of the tower (m)
b= OHGW separation (m)
N_g = GFD (flashes/km^2/year)

N_s =flashes/100km/year

Figure 2.14 illustrates the GFD for Durban to be 5 flashes per kilometre per year. The calculations regarding N_s will be dealt with in and analysed in Chapter 4.

2.8 Methodological approach of the study

The adopted approach includes using an ATP-EMTP programme to conduct an insulation co-ordination study which replicates a 132kV distribution system within 1.5 km of a substation. The study will analyse the interaction of the insulation provided by the surge arresters and arcing horns independent of one another and in conjunction with each other under different transient disturbances with information provided by the Municipality. It is possible to find similar examples of this type of insulation co-ordination study in [4, 17]. In order to further quantify a marked change in breakdown voltage due to a rotational shift in the arcing horns; the relationship between the breakdown voltage and the rotational shift will be investigated. Laboratory testing will assist in quantifying the leader progression model used to simulate flashover in the insulation co-ordination study.

Chapter 3

The breakdown mechanism between rotated arcing horns

The laboratory experiment, which was conducted in conjunction with the insulation co-ordination study, was used to help quantify the breakdown mechanism observed between arcing horns which have been rotated on an insulator arrangement. In order to obtained accurate CFO points for each point of rotation, the insulator arcing horn arrangement was subjected to an up-down type test, the results of which were classified as the U_{50} for each gap setting. The aim of these tests were to observe the flashover mechanism until such a point that the developed leader no longer broke down to the other arcing horn but rather to the fitting which would then become the shortest distance to a grounded point. It is worth noting here that once the leader started to breakdown to the fitting, that the arrangement would function in the same manner as an insulator fitted with a single arcing horn.

3.1 Experimental setup

The experimental procedure took place in the high voltage laboratory at Howard College. The setup utilised a 7 stage Marx generator capable of producing 125kV_{dc} per stage. The fronting and tail resistors and capacitors are setup to produce a 1.2/50 μs impulse. A basic set up of the Marx circuit diagram can be found in Figure 3.1 and the laboratory layout in Figure 3.2 illustrates how the circuit diagram was realised while maintaining appropriate clearances.

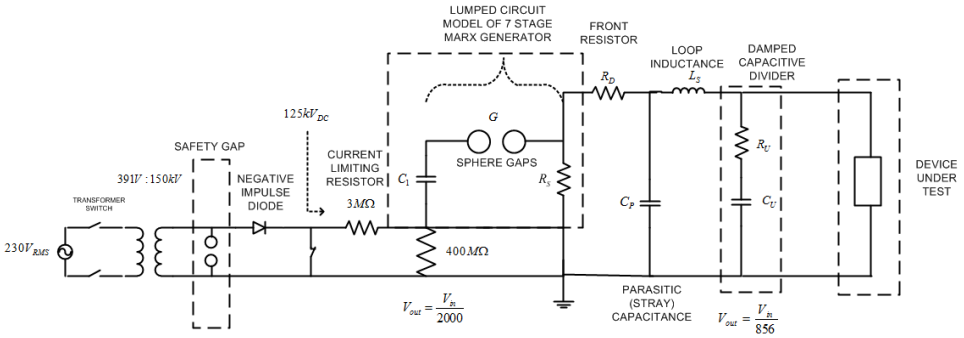

Figure 3.1: Marx generator circuit diagram

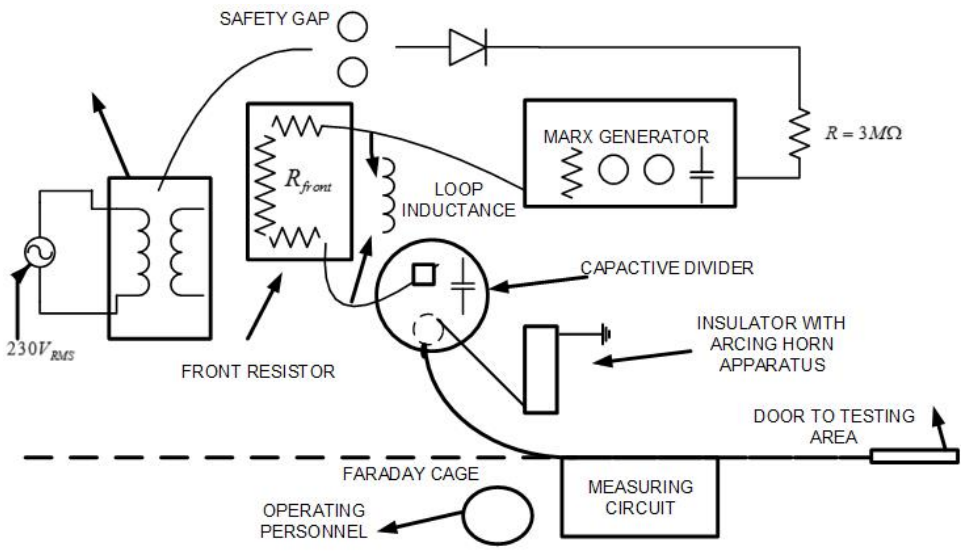

Figure 3.2: Laboratory layout

The arcing horn spark gap was connected to both 88kV and 22kV insulators. The initial arrangement for the 88kV insulator has already been seen in Figure 2.2 and the 22kV setup can be seen in Figure 3.3 below. The horn rotation was measured by placing a ready-made enlarged protractor onto the insulator end fitting after which it was removed so as to not impact the experiment; this was done while maintaining sufficient clearance to the device under test (DUT).

The measurement circuit consisted of a calibrated capacitive voltage divider with a dividing ratio of 856 coupled with an impulse peak measurement system. The impulse peak measurement system had a further dividing ratio and could be attenuated at the point of measurement in steps of 2, 4 or 6 in order to safely read measured values from the laboratory.

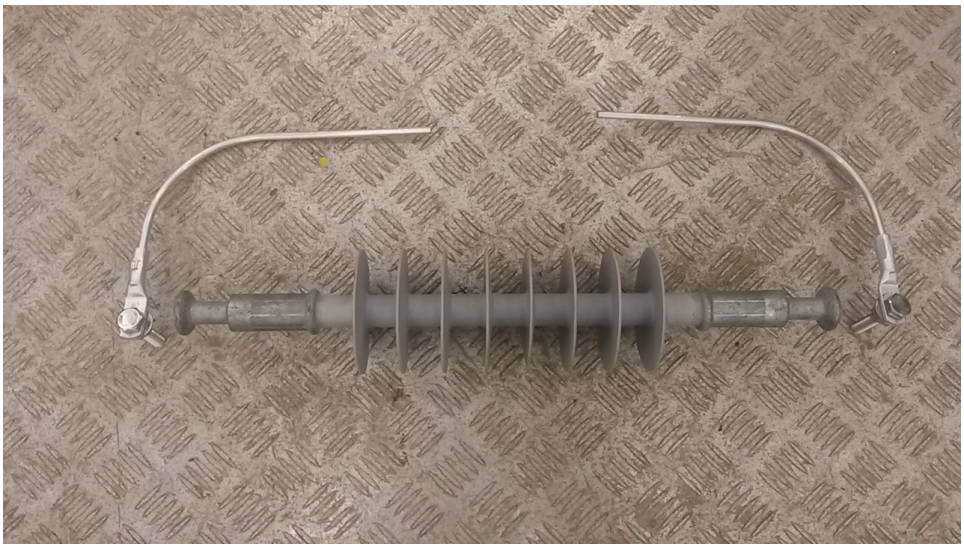

Figure 3.3: 22kV insulator arcing horn apparatus

3.2 Simulating flashover

Much work has gone into the simulation and modelling of flashover. Ab Kadir et al [4] states 4 different methods for modelling flashover namely:

- V-t curves
- The disruptive effect (DE)
- The standard leader progression model (LPM)
- The modified leader progression model

3.2.1 Volt-time curves

It is customary for each piece of equipment to have a characteristic volt-time curve. Transformers, surge arresters and insulator gaps need to be coordinated correctly so as to provide correct margins of safety for costly pieces of equipment. The Figure 3.4 below shows an example of a constructed volt-time curve.

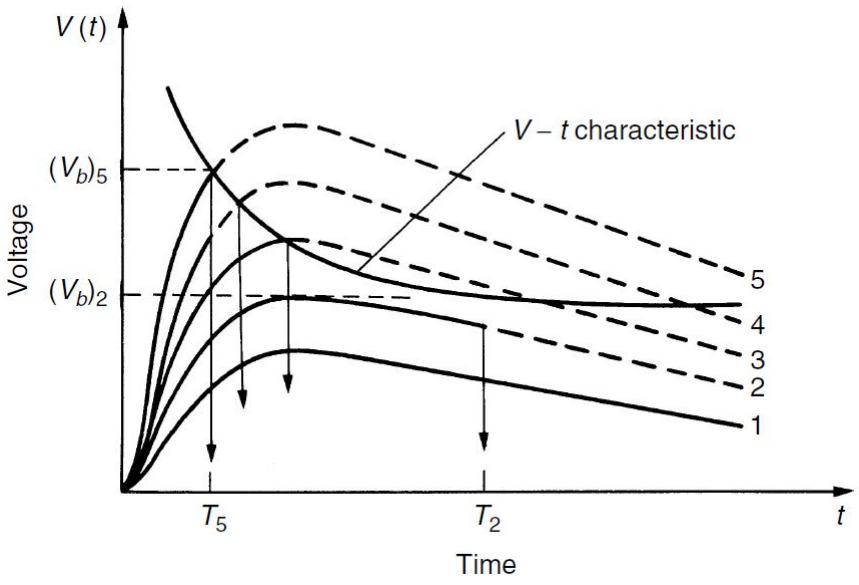

Figure 3.4: Construction of a V-t characteristic curve - taken from [1]

The above curve can be constructed by applying differing amplitude of impulses and recording the time lag to breakdown for each [17]. For a given gap size the breakdown voltage for each point on the V-t curve can be calculated using different values of t. Each amplitude breakdown point and corresponding time are plotted to generate a V-t curve for that piece of equipment. V-t curves have been used to compare results from testing to that found in literature [17].

$$V_{v-t} = a \times L + \frac{b \times L}{t^{0.75}} \tag{3.1}$$

Where a and b are arbitrary constants, L is the length of the gap and t is the time to breakdown.

3.2.2 Disruptive effect (DE)

This method integrates the voltage across a gap above a certain threshold according to the integral in equation (3.2). Once this integral reaches a certain value, flashover is said to have taken place. Simplified versions of this model use V_0 as zero [4].

$$DE = \int (V(t) - V_0)^k dt \tag{3.2}$$

3.2.3 The leader progression model (LPM)

The leader progression model sums up the time taken for the flashover to occur which are namely; the corona inception, streamer propagation and leader propagation. The time to breakdown (t_b) can be expressed as follows:

$$t_b = t_i + t_s + t_l \tag{3.3}$$

Usually it would be necessary to describe each of these time lags in order to describe the LPM more accurately. However, at fairly low voltages, the corona inception voltage is far below the breakdown voltage which leaves it to be a rather irrelevant concept to define. The streamer propagation time can be expressed using the equation found in [4].

$$\frac{1}{t_s} = \frac{1.25 \times E_{max}}{E_{50}} - 0.95 \tag{3.4}$$

where E_{max} is the maximum electric field found in the gap and E_{50} is seen

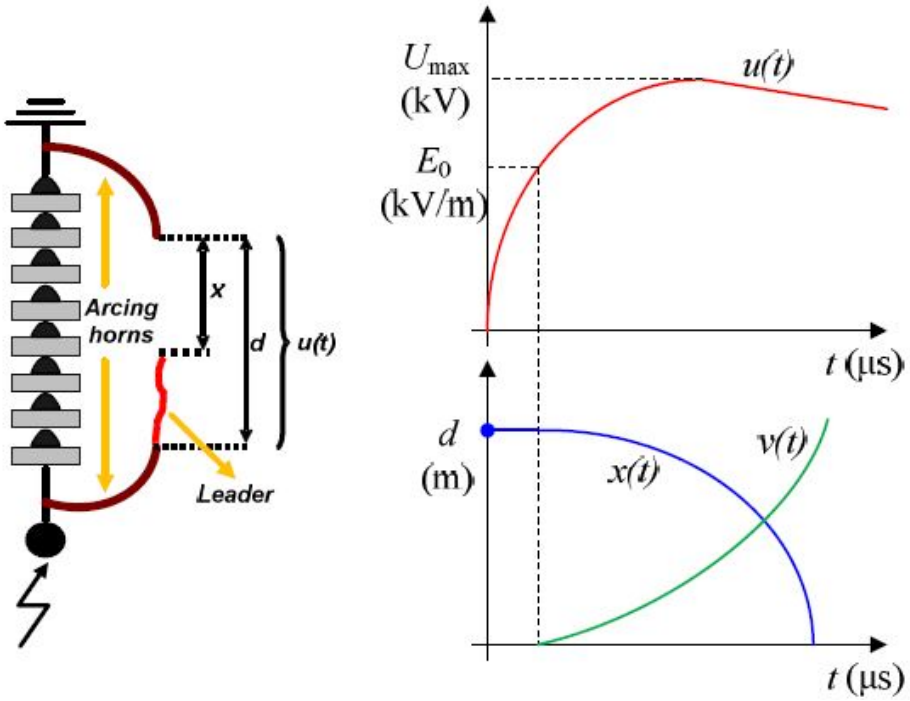

Figure 3.5: Leader progression model - as seen in [3]

to be 500kV/m [18] for a rod-rod model. The leader propagation time can be found by using the following equation for the velocity of the leader for each time step and then calculating the time which it takes to bridge the gap. The equation is as follows:

$$\frac{dl}{dt} = k \times d \times (\frac{U(t)}{d-l} - E_o) \quad (m/s) \tag{3.5}$$

where d is the initial gap distance, l is the leader length at each time step and E_o is the electric field breakdown of air in a rod-rod gap arrangment. The distance travelled can then be found

$$\int \frac{dl}{dt} = x_{leader} \quad (m) \tag{3.6}$$

and the point of backflashover occurs when the following condition is satisfied.

$$x_{leader} > d \tag{3.7}$$

In [3] it was used to compare CFO voltages on high voltage polymer insulators of 110, 120 and 440kV fitted with arcing horns on both ends.
The method can be shown in Figure 3.5 and proceeds in two stages prior to subsequent leader onset.

3.2.4 The modified leader progression model

A modified version of the standard leader progression model can also be utilised using probability distribution for both values K and E_{50} as found in [18]. By using a probability distribution the time to breakdown will vary thereby corresponding to the random nature of the gap breakdown under steep rising impulses. However, in order to ascertain this probability distribution, testing needs to be carried out[4]. For the purposes of this study this approach was not utilised.

3.2.5 Flashover of smaller gaps

Considering the arcing horn arrangements for both insulators, it was noted that the initial gap spacing was less than the minimum distance of 1 metre [18]. It was therefore necessary to include an equation from [19] which governs the spark over voltage for both positive and negative polarity valid for gaps less than 1 meter as shown below where $d_i < 1$m.

$$V_{sp} = 2 + 534 \times d_i \quad (kV) \tag{3.8}$$

3.2.6 Deriving movement

In order to utilise leader progression models to simulate flashover, it is important to derive an equation that governs the size of the spark gap under rotated conditions. It can be assumed that the arcing horn will only substantially rotate in the horizontal plane and far more negligibly in the vertical plane due to its fixed point of origin on the insulator and its rigid bent shape. Therefore, if an initial spark gap distance, x, is presumed and the vertical radius of the arcing horn, r, is given then the arcing horn will be seen to rotate horizontally through an angle θ as shown below.

It can be derived using spherical coordinates that the shortest distance between the arcing horns can be shown to be the following.

$$d_{gap}(x, r, \theta) = \sqrt{(x^2) + (r - rcos\theta)^2 + (rsin\theta)^2} \quad m \tag{3.9}$$

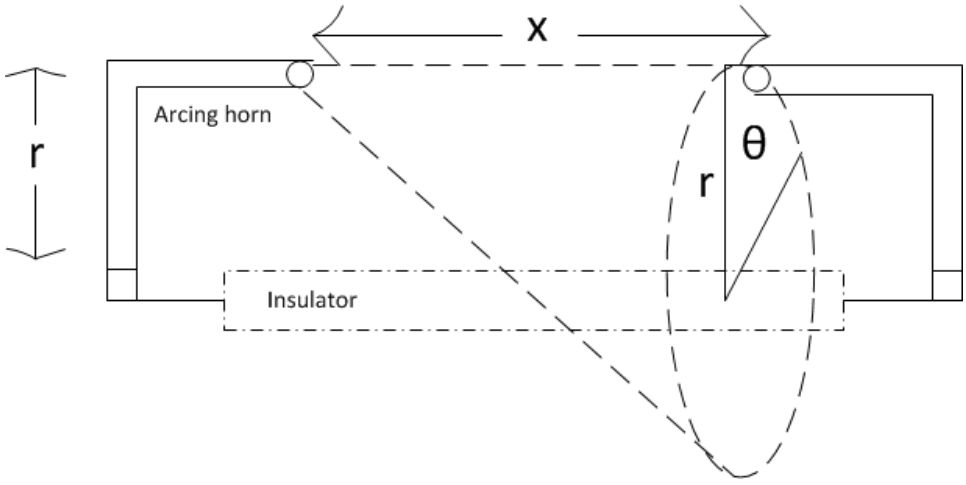

Figure 3.6: Rotated arcing horn arrangement with defined constants

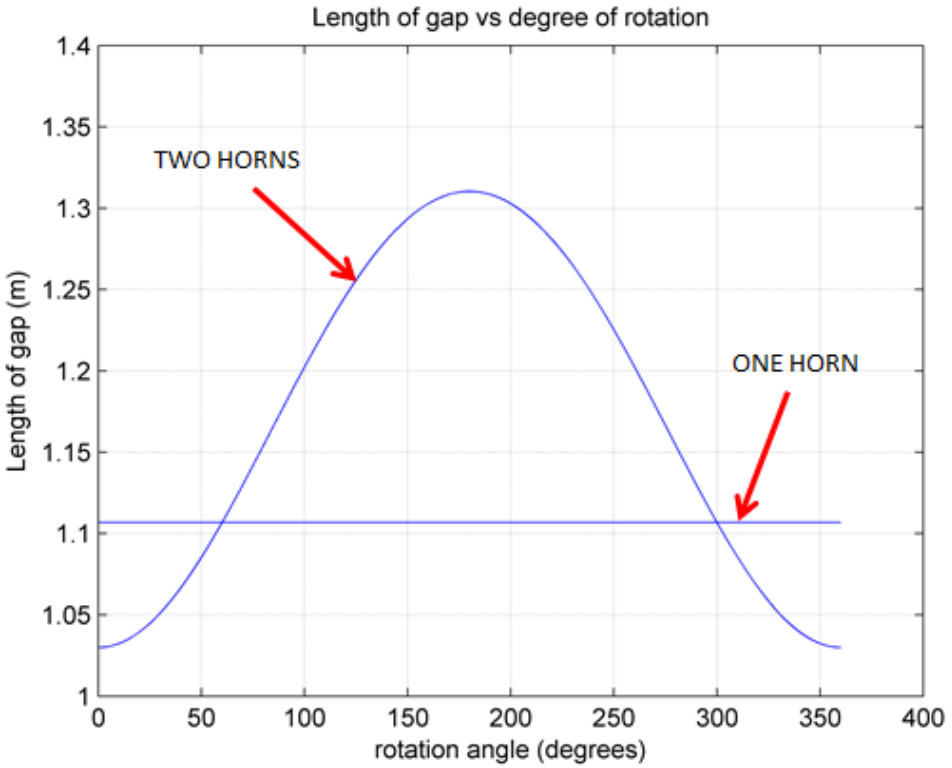

Figure 3.7: Results of rotating arcing horn on 132kV insulator

3.2.7 One arcing horn

It can be observed in the graph that there exists a straight line which intercepts the bell shaped curve at around 60°. This line is the result of applying one arcing horn and calculating the distance to the fitting of the insulator. The following equation is used which is similar to the equation representing two arcing horns.

$$d_{gap}(x, r, \theta) = \sqrt{(x^2) + (rcos\theta)^2 + (rsin\theta)^2} \quad m \tag{3.10}$$

This equation yields the same distance during the full rotation of the arcing horn as it is rotating in a circle with a fixed radius relative to the insulator. Therefore, the shortest path to the end fitting, rather than the arcing horn, occurs at roughly θ= 60°.

3.3 U_{50} calculations

The disruptive discharge on external insulation is dependant on atmospheric conditions.

3.3.1 Humidity correction factor

The humidity correction factor, k , for impulse voltages may be expressed as seen in equation (3.11).

$$k = 1 + 0.01(\frac{h}{\delta} - 11) \tag{3.11}$$

where h represents the absolute humidity and δ the temperature correction factor. For gaps less than 0.5 m however, the humidity correction factor shall not be applied [16].

3.3.2 Air density correction factor

Pressure and temperature perform a role influencing the U_{50} voltage and must be taken into account. Equation (3.12) denotes.

$$\delta = (\frac{b}{b_0}) \times (\frac{273 + t_0}{273 + t}) \tag{3.12}$$

where b_0 is seen to be the standard atmospheric pressure and t_0 the standard room temperature [16], [20].

3.4 U_{50} testing

The insulators were subjected to an up-down test wherein a total of 20 (N) impulse shots were applied to the spark gap with an initial voltage level, V_i. For each flashover, voltage level V_{i-1} was applied and each withstand V_{i+1}. The number of withstands and flashovers were then summed and the U_{50} voltage was then calculated as follows as per the standard [16].

$$U_{50} = \frac{\delta \times k \times (\frac{\sum(n \times V_i)}{N}) \times s_{measure} \times d_{ratio}}{1000} \quad kV \tag{3.13}$$

where $s_{measure}$ is the scaling ratio of the impulse measurement circuit and d_{ratio} represents the capacitive divider.

The results were recorded for both polarities of impulse.

3.5 Results

Two insulators namely, 88kV and 22kV insulators were subjected to up-down U_{50} testing. The result of the testing of smaller insulators was due to laboratory constraints on the size of the sparkgap on the 132kV insulators being too large to cause breakdown. Both insulator sets were fitted with initial arcing horn spark gaps with the gap of the 22kV insulator being constructed in a ratio proportional to that of the dry arc distance between the two fittings of the 88kV insulator.

- 88kV insulator

  Dry arcing distance: 785mm
  Initial arcing horn separation (x): 400mm
  Arcing horn vertical radius (r): 350mm

- 22kV insulator

  Dry arcing distance: 280mm
  Initial arcing horn separation (x) : 150mm
  Arcing horn vertical radius (r): 207mm

The test results found in the laboratory were then compared to the CFO values found using the leader progression model found from the asymptote of the voltage-time curves for each insulator in Figures 3.8 and 3.9. The results were also compared to the equation governing flashover voltages for spark gaps less than 1 metre as seen in equation (3.14).

$$V_{sp} = 2 + 534 \times d \quad kV \tag{3.14}$$

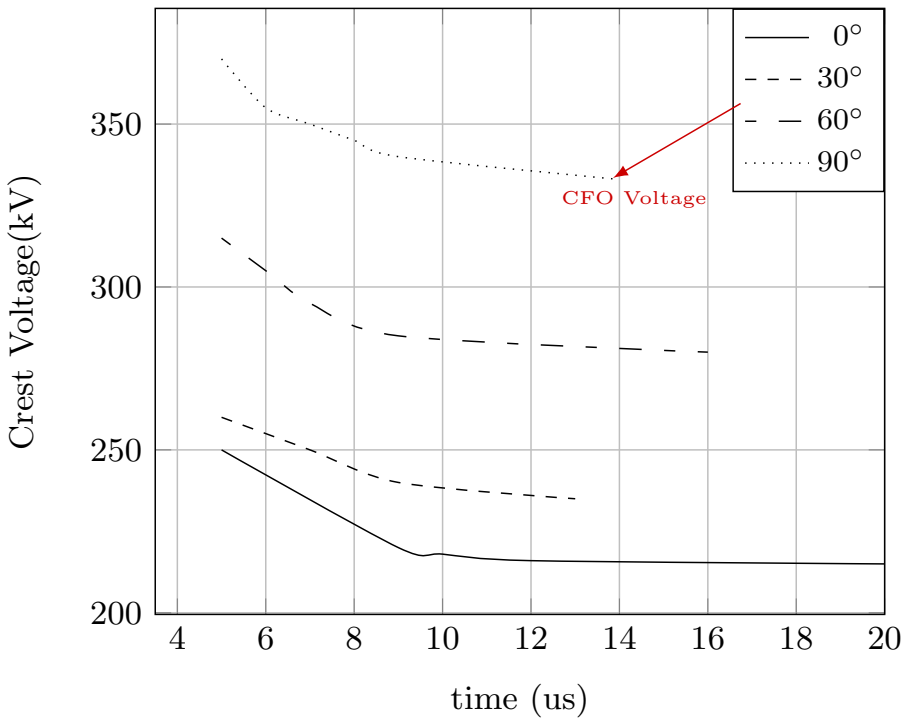

Figure 3.8: V-t curve result for 88kV insulator

Table 3.1: CFO voltage results for 88kV LPM method in Figure 3.8

Rotation (°)	Crest Amplitude (kV)
0	215
30	235
60	280
90	333
One horn	280

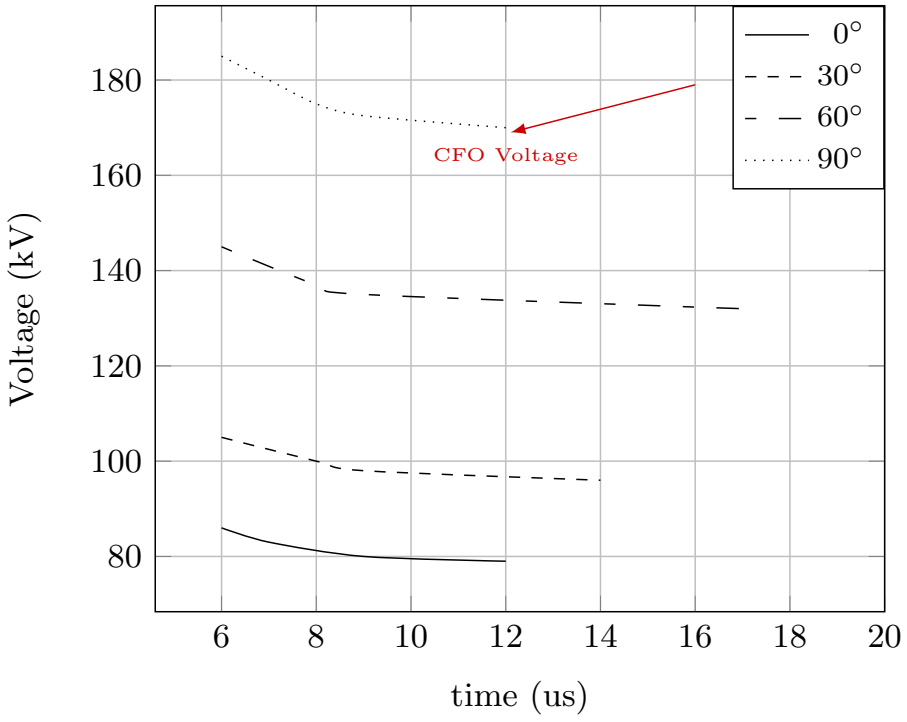

Figure 3.9: V-t curve result for 22kV insulator

Table 3.2: CFO voltage results for 22kV LPM method in Figure 3.9

Rotation (°)	Crest Amplitude (kV)
0	79
30	96
60	132
90	170
One horn	132

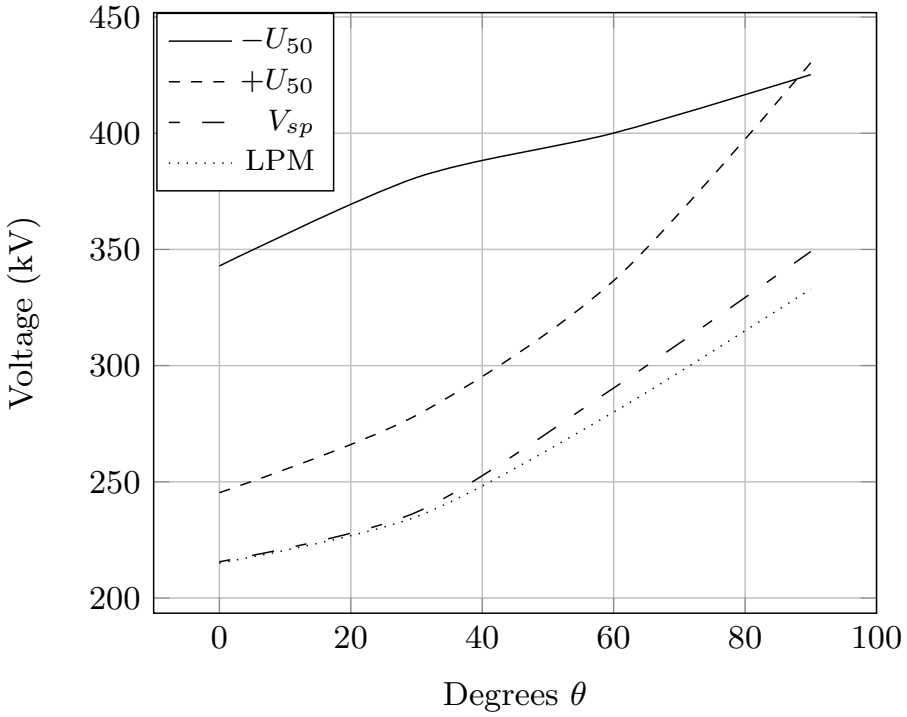

Figure 3.10: Results of 88kV insulator testing

Table 3.3: Voltage results for 88kV laboratory testing in Figure 3.10

Rotation (°)	U_{50-}(kV)	U_{50+}(kV)	V_{sp} (kV)	LPM (kV)
0	343	245	216	215
30	381	279	237	235
60	400	337	290	280
90	425	430	349	333

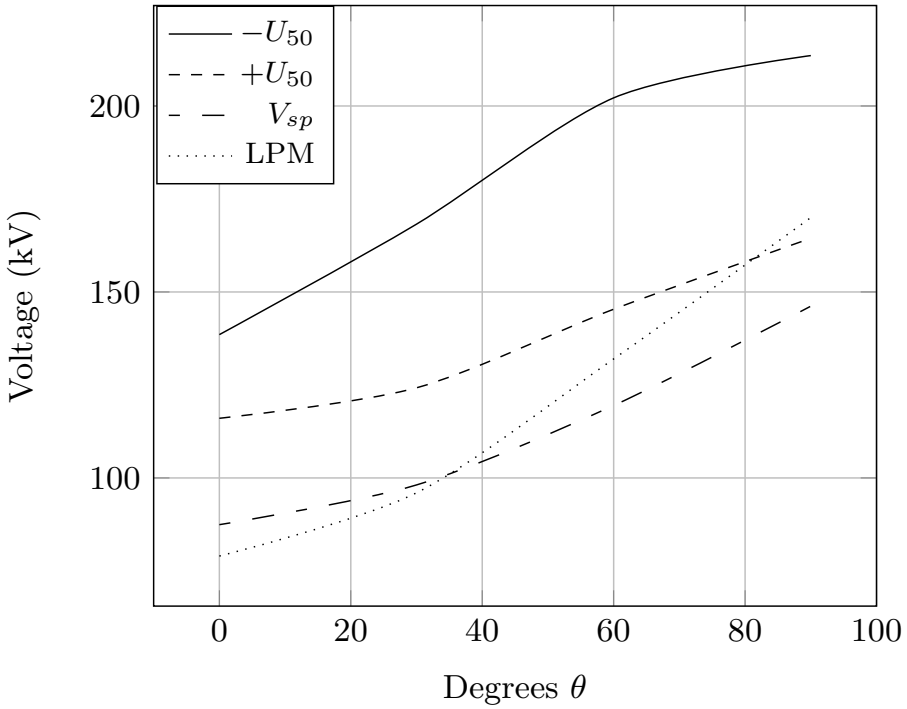

Figure 3.11: Results of 22kV insulator testing

Table 3.4: Voltage results for 22kV laboratory testing in Figure 3.11

Rotation (°)	U_{50-}(kV)	U_{50+}(kV)	V_{sp} (kV)	LPM (kV)
0	139	116	87	79
30	168	124	98	96
60	202	145	119	132
90	214	164	146	170

The results of both the positive and negative impulses across the arcing horn air gap were recorded for rotations up to 90° and compared in the graphs contained in Figure 3.10 and 3.11.

It can be noted from the graph that the negative impulse had a higher U_{50} voltage than the positive impulse for almost all points of rotation. This can be expected as the avalanche mechanism for each polarity differs. The breakdown voltages found from theory for gaps less than 1 metre and the leader progression model (LPM) were calculated to be lower than that of both the positive and negative impulses.

From Tables 3.1 and 3.2 it can be seen that for each of the respective insulator arrangements an angle of 60° denotes the point at which the shortest distance to an earth point becomes the fitting and not the opposing arcing horn. As a result, flashover did not always occur to the opposing arcing horn.

3.5.1 One arcing horn vs. two

It was noticed that not all flashovers were terminating on the opposing arcing horn but rather to the end fitting of the insulator. This was particularly more apparent on the 22kV insulator. A further investigation was set up by means of a U_{50} test which was then conducted on both set ups carrying one arcing horn fitted to the live side. The following results were recorded.

Table 3.5: U_{50} test on an 88kV insulator

	Positive Impulse (kV)	Negative Impulse (kV)
$U_{50single}$	440.98	n/a
$U_{50double@90°}$	430	425

Due to the limits on supply the negative impulse U_{50} voltage could not be attained for the 88kV insulator. The same experiment was conducted on the 22kV insulator.

Table 3.6: U_{50} test on an 22kV insulator

	Positive Impulse (kV)	Negative Impulse (kV)
$U_{50single}$	192.38	221.77
$U_{50double@90°}$	164	214

Figure 3.12: 22kV insulator flashover for one arcing horn to the fitting

3.6 Discussion of results

The laboratory experiment was utilised to ascertain how the theoretical modelling of leader breakdown could be compared to live application; as well as investigating the breakdown mechanism between rotated arcing horns.

It can be noted from the results that use of the LPM and the equation governing spark gaps less than 1 metre revealed lower breakdown voltages for the same gap size. This could possibly be attributed to the presence of the insulator in the test arrangement as [18] and [21] do not incorporate the use of an insulator to attain their respective results. This presence effects the distribution of the electric field around the arcing horns thereby influencing the formation of the avalanche and subsequent streamer and leader breakdown. In order to attempt to incorporate the effect of the insulator an average of the division between the negative and positive laboratory results

with the theoretical results was taken and a factor was found.

$$k_{neg} = \sum_{0^\circ}^{90^\circ}(\frac{U_{50-}}{< 1m}) \tag{3.15}$$

$$k_{pos} = \sum_{0^\circ}^{90^\circ}(\frac{U_{50+}}{< 1m}) \tag{3.16}$$

The values were found to be $k_{neg} = 1.5$ and $k_{pos} = 1.2$. These factors imply that theoretical modelling yields lower values for breakdown and therefore, deems it suitable for modelling the leader breakdown in the insulation coordination study as opposed to having to conduct an up-down test on the 132kV insulator gap.

It is also worth noting the breakdown mechanism, which was seen to change as the arcing horn rotated further away from its initial position with flashes occurring more regularly to the fitting of the insulator. Mathematical calculations yield the shortest distance to the fitting to occur at 60° of rotation, however, the results of the single arcing horn in Tables 3.5 and 3.6 indicate a rejection of the mathematical hypothesis.

In Table 3.5, the U_{50} recorded for the single arcing horn gap is 441kV for a positive impulse whereas for two arcing horns using the same impulse at 90° the value was 430kV. Similar results can be observed on the 22kV insulator albeit occurring slightly earlier. It can thus be concluded that the change in breakdown mechanism occurs closer to 90° as opposed to the original 60° which was hypothesised earlier in the dissertation. This discrepancy can be possibly attributed to the structural differences of both the end fitting and arcing horn and the resulting difference in avalanche and field formation.

As a result the maximum attainable rotation whereby the dry arcing distance is effected will be seen to be 90°. Beyond 90° of rotation however, breakdown across the insulator occurs to the end fitting essentially rendering the second arcing horn redundant, therefore the CFO voltage of the insulator will remain constant for further increments of rotation.

Chapter 4

Investigating the role of arcing horns on 132kV sub-transmission lines

Any insulation co-ordination study must as accurately as possible investigate the magnitudes of overvoltages in the event of flashover on a system as stated in [4, 22]. Should any overvoltages pose a threat to the CFO voltage of any piece of equipment, and therefore the designed BIL of the system, then an element of risk could be imposed. The occurrence of flashover during shielding events predominate over those that occur in the instance of shielding failure as a result of the current striking the phase conductor being too low to cause a flashover. Previous studies of insulation co-ordination cite backflashover [4, 23] as the primary cause for concern in the case where a line is equipped with shield wires in order to attempt to divert the lightning strike away from the phase conductors of a transmission system, however, there is no generic case when dealing with arcing horns.

The insulation co-ordination model seeks to identify the importance of arcing horns within a sub-transmission system. Adverse weather conditions possess the means to rotate these arcing horns through an angle thereby subjecting the insulator and the system to the possibility of damage in the event of an overvoltage event such as lightning. The model comprises of a single circuit transmission line spanning the length of 1.5 km before a substation. The eThekwini 132kV transmission system utilises two arcing horns on either

end of the insulator within 3 span lengths of the substation, as well as single arcing horn arrangements, coupled with corona rings and other secondary connecting apparatus to evenly distribute electric fields at the end fittings.

4.1 Arcing horn gap setting

The spark gap formed by the arcing horn can be seen to be part of the insulation of the system as it provides a secondary means to divert surge current to earth, the primary means being via that of the surge arrester. According to [24], rod-rod or spark gaps are set at a voltage well lower than that of the substation equipment which is being protected as the insulation is self restoring. These insulating gaps however, can often be disadvantageous and impact the system in the following manner:

- When the gap operates a short circuit is formed to earth resulting in the system requiring to clear the earth fault.
- Gap operation can result in steep $\frac{dv}{dt}$ changes which can potentially stress transformer inter-turn insulation.
- A spark gap has a slow response to waveforms with a fast rise time and is influenced by polarity of the surge as well as atmospheric conditions.
- Smaller gaps are susceptible to maloperation due to wind, wind-borne debris and birds.

Studies have cited the arcing horn spark gap as an important aspect of insulation co-ordination [25], however, although there have been many studies which consider breakdown in air gaps such as those in [9, 26], there are none which are specific in the context of rotated arcing horns.

4.2 Surge Arresters

Surge arresters are located in the nearby vicinity to a transformer, in order to protect it from overvoltages. In selection of the surge arrester it is important to note the types of transients which occur most on the system in order to limit the probability that damage will occur to insulation located in the station. It can be noted from [27] that it is necessary to:

- Develop a margin between the voltage rating of the system and the voltage of the lightning arrester.
- The voltage difference between the lightning arrester rating and its corresponding surge discharge voltage.
- A safety margin between the protective level of the lightning arrester and the insulation level of the equipment.

Surge arresters perform a vital role in insulation co-ordination as they provide a path to divert current to ground at high voltage levels. They are prominently utilised and many studies exist demonstrating their importance such as those found in [28, 8, 23].

4.3 Occurrence of backflashover

Backflashover (BFO) was defined in Chapter 2 as a discharge completed from an earthed support to an energised conductor which occurs as a result of a lighting strike intercepting a transmission tower or shield line [4]. The combination of the surge impedance of the tower structure, as well as the reflection co-efficients formed with the earth resistance result in a potential of the cross arms of the tower being raised. When a lightning surge current strikes the tower top, current is diverted along the shield wires to adjacent towers and some of the transient waveform is diverted to earth. The essence of backflashover can be illustrated in Figure 4.1.

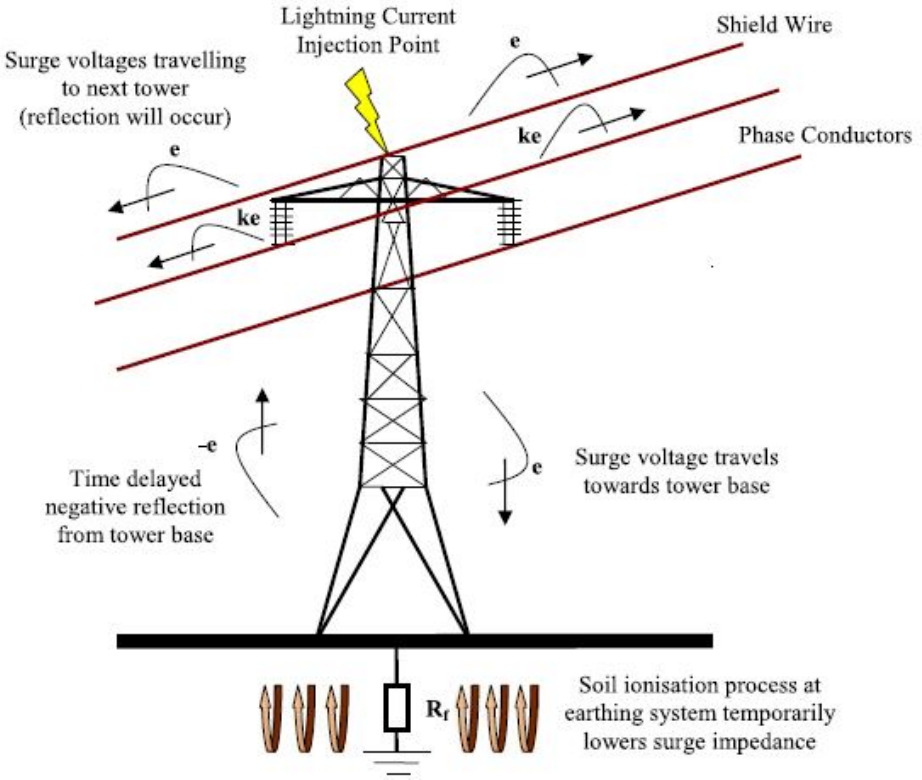

Figure 4.1: Backflashover process on a transmission tower - taken from [4]

The voltage that can be observed at the tower top, as described by [10], is governed by the Z_T, the surge impedance of the tower, Z_g the surge impedance of the ground wire and the amplitude of the lightning stroke, I_{stroke} :

$$V_{top} = \frac{Z_T \times Z_g}{Z_g + 2Z_T} \times I_{stroke} \tag{4.1}$$

however, a number of events may take place to reduce the voltage observed at the top of the tower. These events may include:

- The electromagnetic coupling of the shield wires with that of the conductors can result in a portion of the voltage being observed on the phase conductor.
- Depending on the travel time, the reflections of the earthing resistance and soil ionisation can result in the voltage being reduced across the insulator string.

- Reflections from other towers may also result in destructive interference of the voltage across the string although, due to the travel time this is usually insignificant.

4.3.1 Factors promoting backflashover

There are a number of aspects which influence BFO on high voltage transmission lines. [29, 30, 14, 15]. They include [31]:

- Poor earthing of transmission towers: Earthing of transmission line towers performs a pivotal role in their protection. Grounding resistances in excess of 100Ω may require the installation of transmission line surge arresters (TLSA).
- Ineffective shielding: Perfect shielding of phase conductors only permits lightning currents of low amplitude to strike them thus deferring most strikes onto shielding wires or transmission towers.
- Positioning of TLSA: Should they be required, the positioning of TLSA can greatly inhibit the effect of backflashover.

4.3.2 Probability analysis of backflashover

There have been multiple studies which have been conducted a probability analysis of lightning causing a flashover to a transmission system, such as those found in [4, 17]. The studies have used equations in order to calculate the number of flashes received to a line in an area given the number of thunderstorm days in a year, TD, and the ground flash density, N_g. The following equation can then be applied to determine the probability of a particular amplitude of lightning current occurring.

$$p(I > I_c) = \frac{1}{1 + (\frac{I}{I_c})^{2.6}} \tag{4.2}$$

with mean lightning current amplitude, $I_c = 31$ kA [11]. The frequency of BFO can be calculated by knowing the flash density for a given area, N_s and the probability distribution of lightning current amplitude:

$$BFO_{rate} = 0.6 \times N_s \times p(I) \tag{4.3}$$

4.4 The model

An insulation co-ordination model of a 132kV sub-transmission system was constructed in ATP-EMTP using various different standards and nominal values. The system which is made up of 3 transmission towers and separated by 3 spans of transmission line with a length of 0.5 km; originates from a 132kV source and terminates in a step down 132kV - 11kV substation. Figure 4.2 illustrates the basic layout of the modelled system.

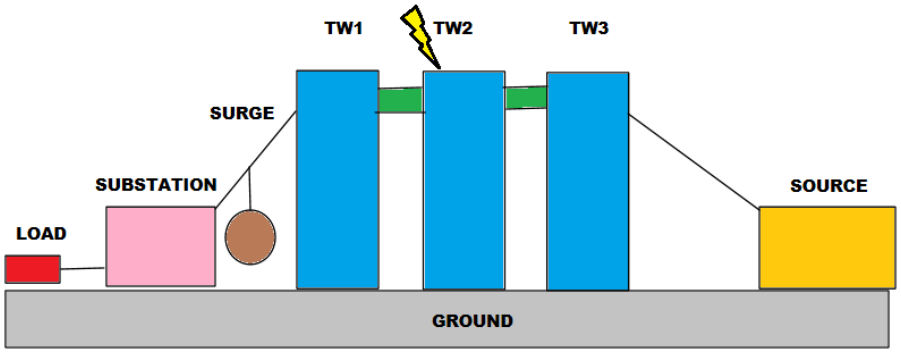

Figure 4.2: System modelled

4.5 Transmission towers

4.5.1 Surge impedance of towers

The typical transmission tower has a height that is quite large in comparison to the rise time of some of the components of lightning strokes. The role that the tower plays in the behaviour of a transmission system under surge duress can be modelled as follows:

1. It can be considered as a series of lumped circuit elements usually determined by inductances.

2. It can be modelled by a short transmission line segment with a constant or variable surge impedance

3. It can be modelled as a series of electromagnetically coupled objects.

In order to correctly calculate the surge impedances on the line, the travel time, ν, must be known or assumed to be the speed of light or 3×10^8 $m.s^{-1}$. Once the travel time is well defined it is possible to calculate the respective inductances and capacitances using equation (4.4) in combination with (4.5).

$$Z_{Tk/Ak} = \sqrt{\frac{L}{C}} \tag{4.4}$$

$$\nu = \frac{1}{\sqrt{LC}} \tag{4.5}$$

In order to accurately predict the behaviour of a transmission tower under the influence of a lightning strike the equivalent tower surge impedance model must be accurately calculated. The tower model as shown in Figure 4.3 should be divided into four sections and the respective surge impedances calculated for the tower structure itself, the bracings and the cross arms using the following formulae found below.

The surge impedance of each section Z_{T1},Z_{T2} etc. can be expressed as:

$$Z_{Tk} = 60 \times ln[(2\sqrt{2} \times \frac{h_k}{r_{ek}}) - 2] \quad \Omega \quad k = 1, 2, 3, 4... \tag{4.6}$$

Additionally, the expression for tower cross arms:

$$Z_{Ak} = 60 \times ln(\frac{2h_k}{r_{Ak}}) \quad \Omega \quad k = 1, 2, 3, 4... \tag{4.7}$$

where r_{ek} and r_{Ak} represent the equivalent section length and equivalent radius of cross arm respectively for each value of $k = 1, 2, 3...$ The sub-transmission towers were modelled according to [5]. Relevant equations were used to model the cross arms and each tower section independently. This method of surge impedance modelling is widely recognised as noted in [15] and [29]. Table 4.1 shows the calculated values for the surge impedances and the basic tower dimensions can be found in Appendix B.

4.6 The reflection co-efficient

Should there exist a steep change in geometry from a surge moving from one medium to another this could result in a change in surge impedance. An example of this phenomenon can be found when a lightning current

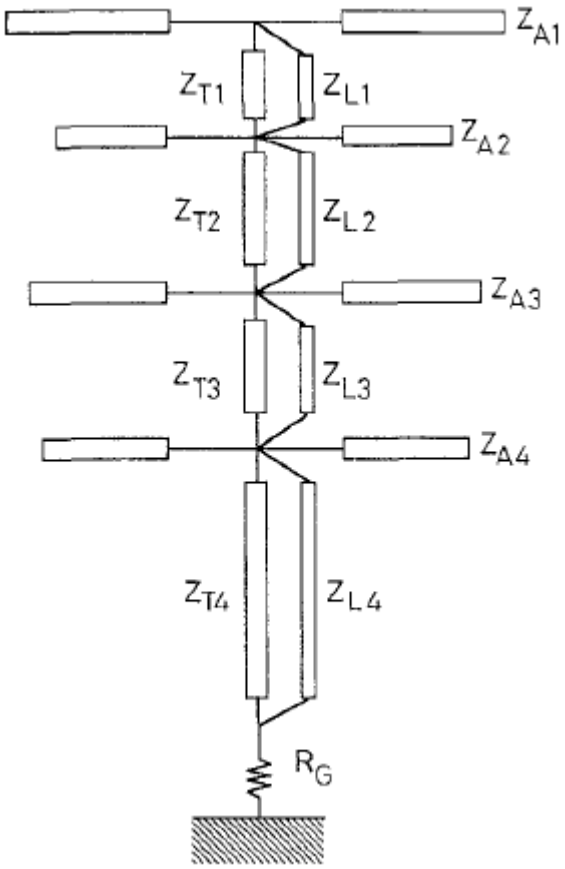

Figure 4.3: Equivalent distributed model of a transmission tower as found in [5]

Table 4.1: Surge impedances for modelled transmission tower

Z_{T1}	167 Ω	Z_{A1}	287 Ω
Z_{T2}	161 Ω	Z_{A2}	282 Ω
Z_{T3}	157 Ω	Z_{A3}	279 Ω
Z_{T4}	152 Ω		

moves along a transmission line and encounters a transmission tower; the voltages and currents will change on both sides of the interface and a certain magnitude will be reflected back, thereby lowering the voltage. A reflection

co-efficient can be calculated as follows:

$$\rho_{12} = \frac{Z_2 - Z_1}{Z_2 + Z_1} \tag{4.8}$$

The reflection of a surge waveform moving from Z_2 toward Z_1 has the reflection co-efficient ρ_{21} which is not the same as ρ_{12}. The voltage on both sides of the interface is constant and the sum of the currents moving toward the interface should be zero. The relationship between the surge impedances and the reflection co-efficients can also then be defined:

$$Z_2 = \frac{1 + \rho_{12}}{1 - \rho_{12}} \tag{4.9}$$

4.7 Transmission lines

The transmission lines bundles were modelled using zebra and rabbit dimensions for the conductor and shield wires respectively. The relevant specifications can be found in below:

- Zebra
  → diameter: 28.62mm
  → Ω/km : 0.06740

- Rabbit
  → diameter: 10.05mm
  → Ω/km : 0.5426

4.7.1 Surge impedance and surge frequency bandwidth

Analysis has been done on transmission lines in response to lightning currents. The equivalent bandwidth can be computed through two expressions as found in [15]; this change in bandwidth requires the correct transmission line modelling to be used, namely; the JMarti frequency dependant model.

$$f = \frac{0.35}{t_{90\%} - t_{10\%}} \quad Hz \quad or \tag{4.10}$$

$$f = \frac{dI/dt}{2\pi \hat{I}} \quad Hz \tag{4.11}$$

4.7.2 JMarti frequency dependant model

The skin effect was implemented and the transmission lines were modelled using the frequency dependant JMARTI model found in [32]. This model was preferred over the PI and Bergeron models due to the nature of lightning and the changing bandwidth.

4.8 Earth resistance

The earthing of the transmission tower was varied between values 10Ω to 30Ω in order to ascertain the effect on BFO probability. Using a constant value of earth resistance is an accepted method for modelling purposes as mentioned by [11] and therefore it was deemed acceptable for the study.

4.9 Insulator characteristics

Polymeric longrod 132kV insulators with dimensions as specified by the eThekwini Municipality were used. The dry arcing distance was modelled to be controlled by the arcing horns. A sample drawing can be found in Appendix B.

4.10 Substation

The 132-11kV step down substation was modelled using two surge arresters to protect both the transformer as well as the measuring current and voltage transformers. A yard layout can be found in Figure 4.4. Suitable values for the current transformer (CT), circuit breaker (CB) and the apparatus connections (AC) were found in [33] and are tabulated in Table 4.2

Table 4.2: Substation equipment values

Current transformer	250 pF
Post insulator	80 pF
Circuit breaker	100 pF
Apparatus connection	1 μH/m

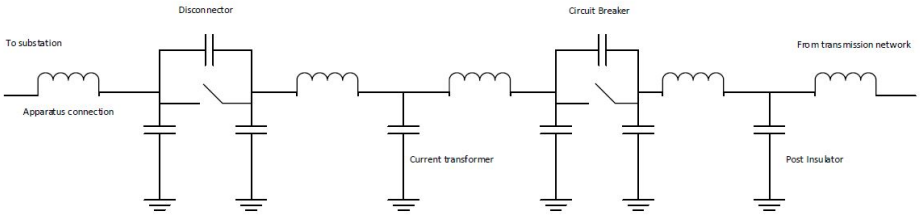

Figure 4.4: Substation model

4.11 Surge arrester modelling

A surge arrester was modelled in order to prevent transients from entering both the substation and the transformer. The modelling was based on the work done by the IEEE Working Group (WG) 3.4.11 [34]. The circuit

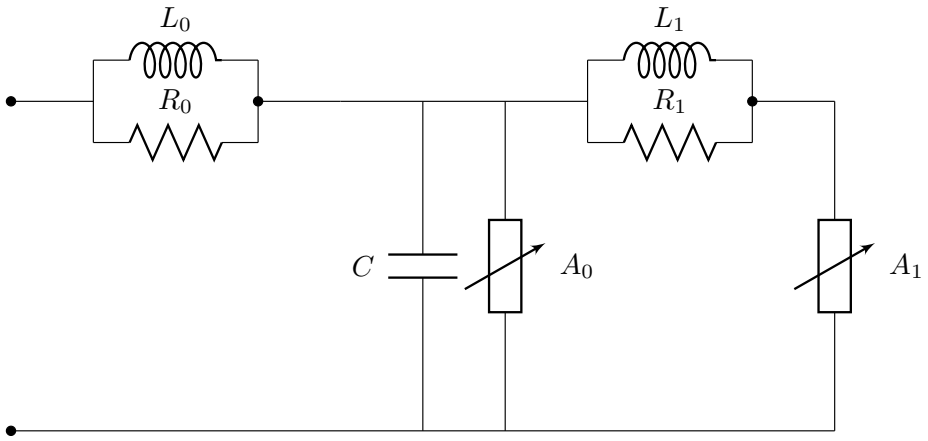

Figure 4.5: Model of surge arrester

elements in Figure 4.5 were based largely on physical dimensions of the arrester found on the ABB website.

$$L_1 = \frac{15d}{n} \quad mH \tag{4.12}$$

$$R_1 = \frac{65d}{n} \quad \Omega \tag{4.13}$$

$$L_o = \frac{0.2d}{n} \quad mH \tag{4.14}$$

$$R_1 = \frac{100d}{n} \quad \Omega \tag{4.15}$$

$$C = \frac{100n}{d} \quad pF \tag{4.16}$$

where d is the estimated height of the arrester in meters and n is the number of parallel columns in the arrester. The zinc oxide surge arrester chosen had a height d = 1.584m and two parallel columns, therefore, n = 4. The calculated values can be found in Table 4.3

Table 4.3: Arrester circuit values

L_1	5.9 mH
R_1	25.7 Ω
L_0	0.08 mH
R_1	39.6 Ω
C	252.5 pF

In order to verify the workings of the model two current waveforms were applied to the arrester, namely; a 8x20 at 10kA and a 30x60 at 1kA. The results of the residual voltage vs. time are shown below in Figures 4.6 and 4.7

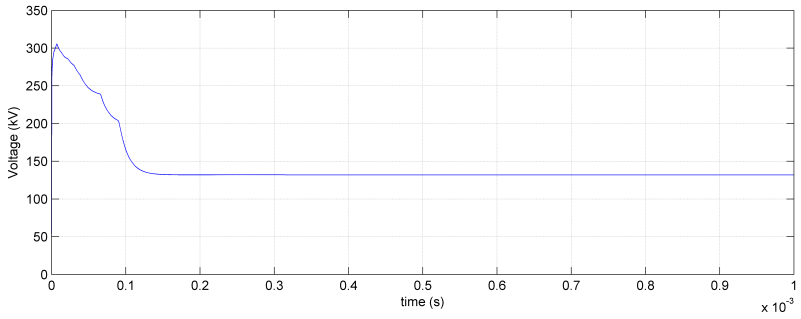

Figure 4.6: Residual voltage for a 10kA, 8x20μs waveform

The two waveforms correspond to the maximum residual voltage of the arrester for both the 8/20 μs condition of a maximum residual voltage of 311kV and the switching 30/60 μs waveform with a maximum residual voltage of 262kV as specified in the datasheet found in [35]. Figure 4.8 illustrates the IV characteristic for the surge arrester ensuring that the time to crest of current precedes the voltage.

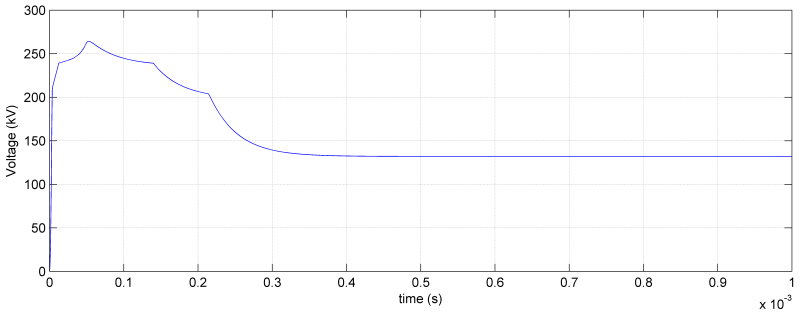

Figure 4.7: Residual voltage for a 1kA, 30x60μs waveform

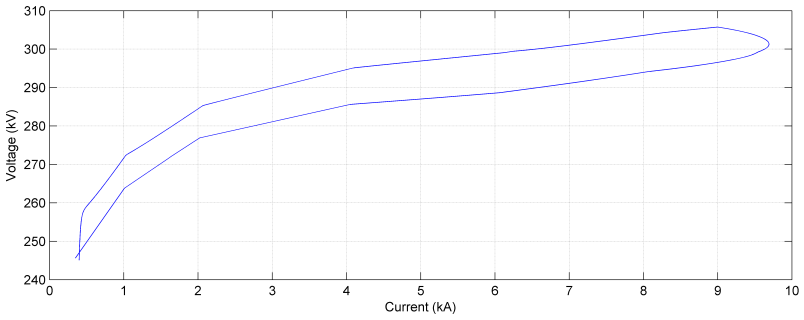

Figure 4.8: Arrester voltage-current characteristic for a 8x20μs impulse

4.12 Transformer

The transformer was modelled using a hybrid transformer model in order to simulate the capacitive and inductive characteristics as well as the impedance drop across it. Typical values were found in the ATP-EMTP environment for capacitance and inductance and a percentage drop across the resistance. These values can be found within the frequency of transient recovery voltage from IEEE Std. C37.011-1994 - TRV Fig. B.2 as seen in [36]. The primary and secondary windings were connected in delta-star formation respectively with the secondary winding solidly grounded through a resistor as specified in the eThekwini standards [13].

4.13 Results

ATP-EMTP was used to model the different elements in the system.

Figure 4.9 illustrates a transmission tower modelled with surge impedances with a potential difference measurement probe representing the 132kV insulator strings.

A lightning impulse characterised by a current source was used to simulate a strike to the shield wire of each tower. The system was then iterated through different values of both of earth resistance and current amplitude. Voltages across the insulator strings as well as those voltages entering the substation and insulator were monitored.

Figure 4.10 illustrates the effect of ground resistance on the voltage across an insulator string on a transmission tower which is directly effected by the strike to the shield wire.

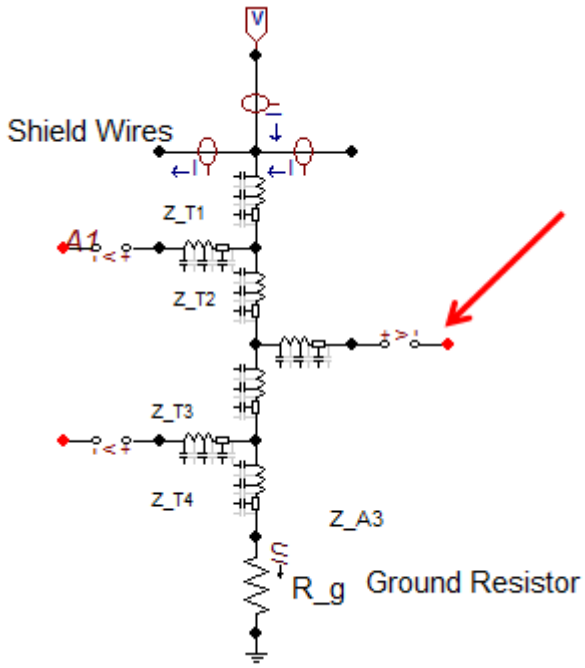

Figure 4.9: Transmission tower modelled in ATP-EMTP

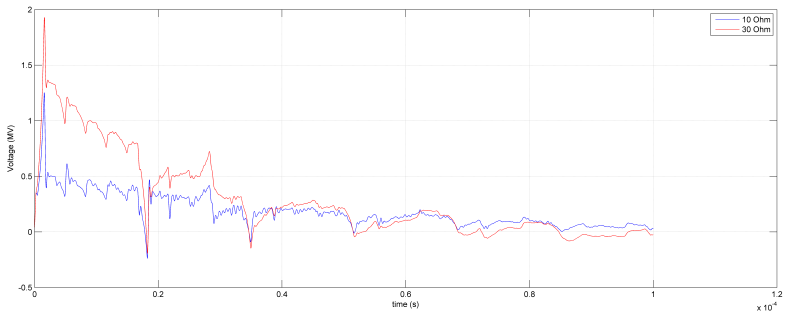

Figure 4.10: Voltages across insulator strings vs. earth resistance

The voltages from the insulator strings of each tower were passed into the LPM which was run in MATLAB. The lightning current was only imposed on one tower at any given time. The LPM was programmed to iterate the length of the leader for the given voltages. Once $x_{leader} > d$ the LPM immediately stored the time to breakdown, the voltage at which breakdown occurred as well as the point of rotation. The process is illustrated by the flow diagram in Figure 4.11.

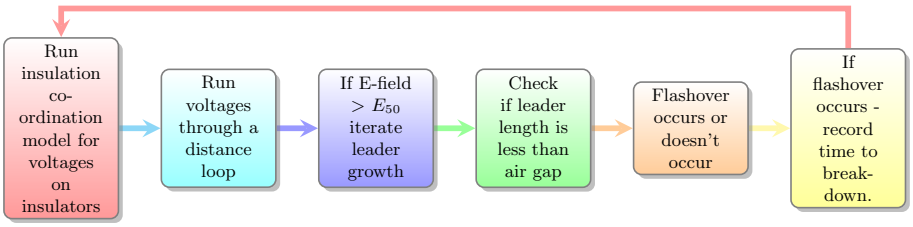

Figure 4.11: Flow diagram outlining V-t curve plotting process

The iteration of both the model and LPM allowed for the plotting of the graph in Figure 4.12 which illustrates the current amplitude required to cause backflashover for a certain degree of arcing horn rotation and earth resistance. Although plotted up to 180° the graph is only valid up to 90°; this was done as a result of the findings in Chapter 3 where flashover in the laboratory was seen to occur to the insulator fitting. Thus, it would be inaccurate to assume the dry arc distance would increase and require an increased current amplitude to cause breakdown.

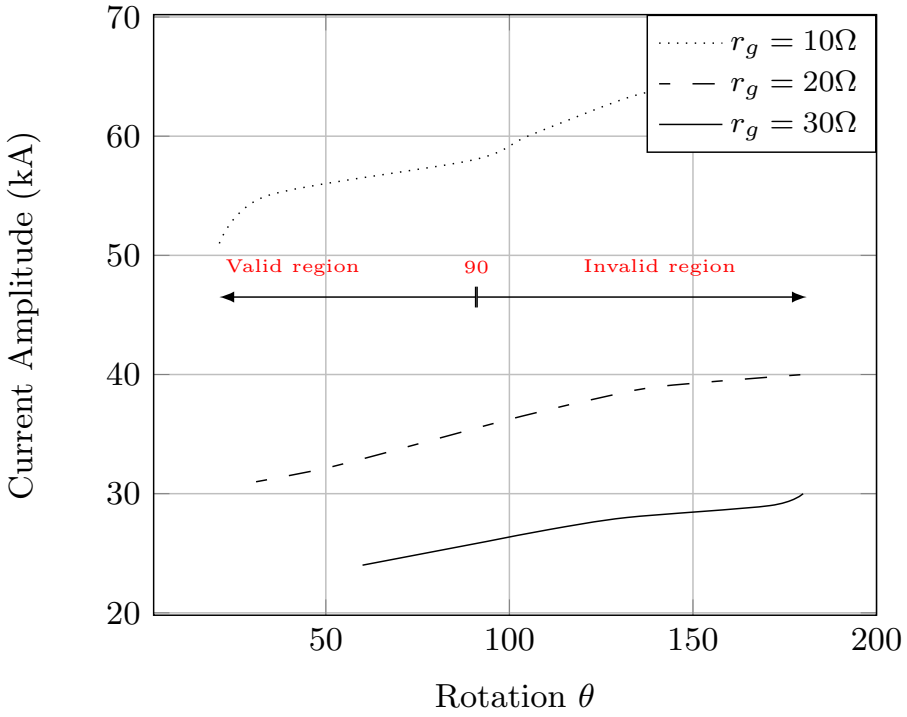

Figure 4.12: Arcing horn rotation vs. lightning current amplitude

Using the results from Figure 4.12, Figure 4.13 could be plotted. This graph outlines the probability of a lightning strike occurring with a current amplitude greater than that value found on the x-axis. This was done by using equation (4.2). This probability was compared to both earth resistance as well as arcing horn rotation. By observing Figure 4.13, it can be seen that for a transmission tower with an earth resistance of 10 Ω and a 0° rotation a 51kA strike would be required to cause backflashover. This according to Figure 4.13, has a 22% chance of occurring. Similarly, to Figure 4.12, a valid and invalid region exists; therefore, for a rotation of 90° which requires a 58kA strike to cause backflashover, the associated probability would be as low as 18%.

The results plotted in Figure 4.13 can be used to find the rate of BFO using equation (4.3) and the number of strikes to 100km of the line using equation (2.13). Thus, the number of lightning strikes which cause backflashover

can be attained. The ground flash density for the greater eThekwini region, which was discussed in Section 2.7.2, can be seen to be 5 flashes/km^2/year. The results can be found in Table 4.4 and are plotted in Figure 4.14.

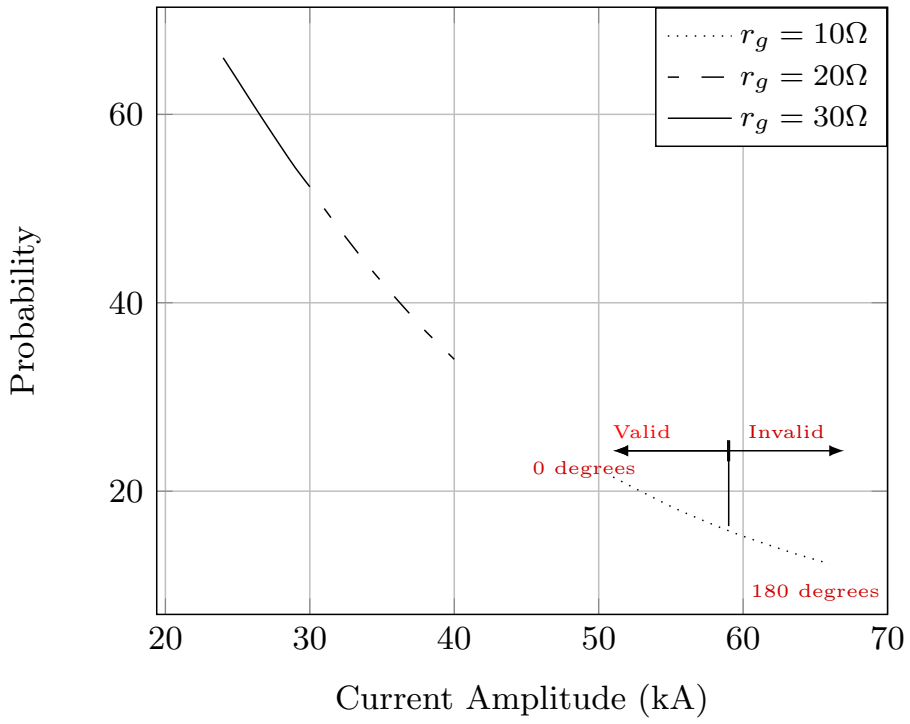

Figure 4.13: Current amplitude vs. Probability

Table 4.4: Rate of BFO vs. earth resistance vs. degree of rotation

Earth resistance (Ω)	Degree of rotation(°)	p(I)	BFO rate (flashes/100km/year)
10	0	0.23	≈ 16
10	90	0.18	≈ 12
20	0	0.5	≈ 34
20	90	0.35	≈ 24
30	0	0.65	≈ 44
30	90	0.55	≈ 37

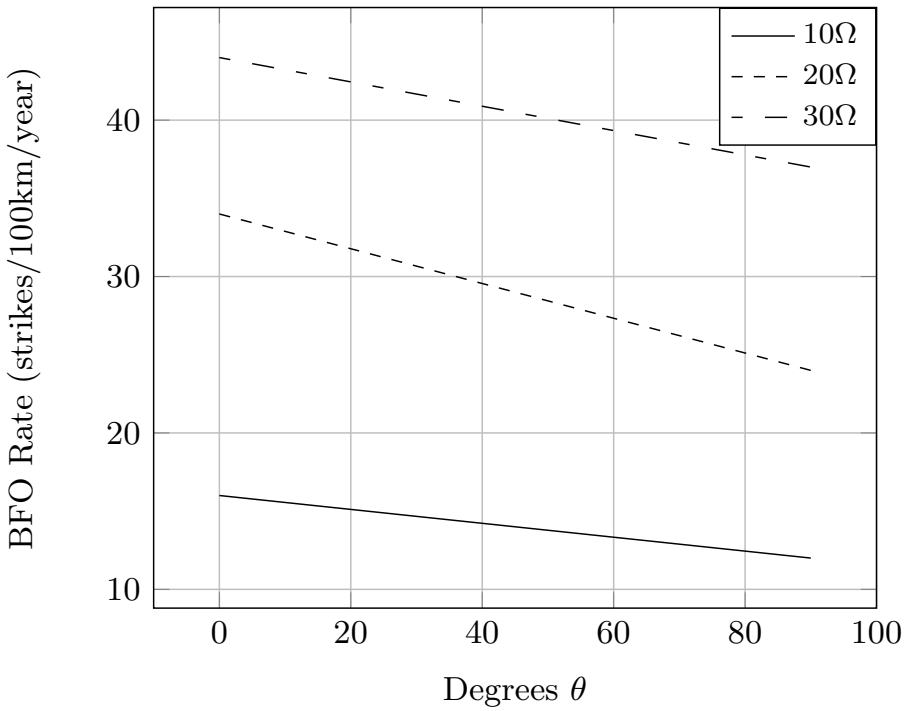

Figure 4.14: BFO rate vs. arcing horn rotation

Figure 4.14 illustrates the values from Table 4.4 for the respective values of earth resistance and degree of rotation. A decrease of the BFO rate can be observed for a higher degree of rotation.

In addition to the ATP-EMTP model the V-t curves were plotted for a 132kV insulator in accordance with method cited in [17]; each point on the graph being determined by using the LPM while adjusting the crest amplitude and recording the time to breakdown.

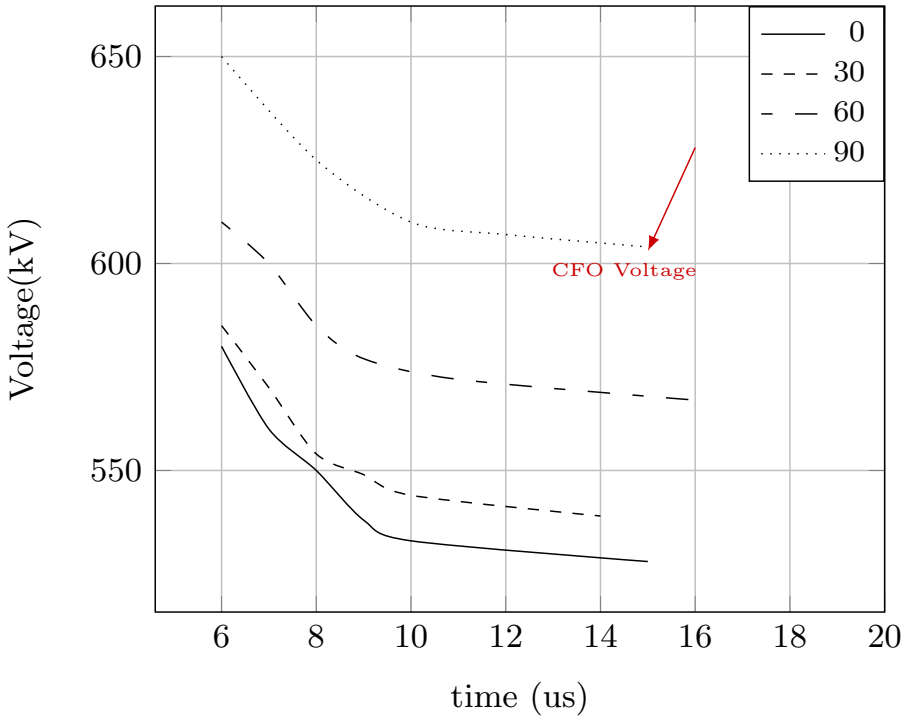

Figure 4.15: 132kV rotated arcing horn V-t curves

Figure 3.7 shows how the spark gap on 132kV insulators fitted arcing horns varies with rotation. At 0° the gap setting is d = 1.03 m, however, at the furtherest angle away of 180° the gap size is seen to increase to 1.3 m. Figure 4.15 shows the V-t curves for 132kV for different degrees of rotation. The CFO voltage can be found from the asymptote of each curve and the values can be found in the Table 4.5.

Table 4.5: CFO voltage results for 132kV LPM method in Figure 4.15

Rotation (°)	Crest Amplitude (kV)
0	528
30	539
60	567
90	604

For the 90° gap it can be seen that the CFO voltage encroaches on the 650kV BIL of the transformer. This could possibly effect the integrity of the system's insulation co-ordination. It is also worth noting the IEEE 4 standards [21] and the corresponding voltages required for both positive and negative polarities to break down gaps of this length. For a 130 cm gap (1.3 m) the breakdown voltage would be rated between 735kV and 850kV for a positive impulse and between 835kV and 965kV for a negative impulse. The table of the standard can be found in the Appendix C.

4.14 Discussion of results

The insulation co-ordination model was conducted in conjunction with the results of the laboratory experiment. The results of the insulation co-ordination study illustrate the comparison between two criteria namely; gap-coordination and earthing resistance.

A rotational shift of either arcing horn relative to one another results in a larger gap in which backflashover takes place; this, coupled with the effect of grounding resistance can greatly influence the theoretical protection of a system against backflashover and subsequent earth faults.

Figure 4.13 which details the probability of a flashover occurring given a set value of earth resistance shows that the system protection against lightning currents as large as 60kA can be greater than 80% provided that the earthing resistance be kept low.

It is clear to observe that earthing resistance plays a vital role in the performance of transmission towers against backflashover. It should also be

noted that the rotation of the arcing horns causes a change in the current amplitude required to cause flashover and the corresponding probabilities of lightning occurrence.

With respect to the effect on the insulation co-ordination, voltages arriving at the transformer were therefore not be in direct danger of causing damage to the insulation as the BIL of the transformer exceed the overvoltages. Even in the worst case scenario with a ground resistance 30Ω and lightning current impulse of I = 66kA the maximum overvoltage reaching the terminals of the transformer was approximately 300kV. The surge arresters installed in the model performed the role of suppressing the overvoltages reaching the transformer by diverting the current to ground, despite the induced overvoltages on the phase conductors being less than those in the event of a shielding failure.

It can also be noted that at a rotation of 90° the V-t curve possesses a CFO voltage value of 604kV which could influence the insulation co-ordination of the system.

Chapter 5

Conclusions and Recommendations

The findings and conclusions of the dissertation are summarised and recommendations for future work are given.

The culmination of the results allows for a number of conclusions to be drawn of which all lead to a better understanding of both the theoretical insulation model and the laboratory flashover experiment with rotated arcing horns fitted onto insulators. To summarise, the following conclusions are drawn:

- Arcing horns are fitted to protect the integrity of the insulator core, sheds as well as end fittings. They also could be seen to perform a role in insulation co-ordination.
- When rotated in the laboratory, the dry arc distance varied and resulted in higher CFO voltages. When the rotation reached 90°, flashover occurred to the end fitting of the insulator instead of the opposing arcing horn.
- For both insulators the CFO voltages for the negative polarity impulse were higher; this can be attributed to the different development of the respective avalanches found in [29].
- The breakdown mechanism between rotated arcing horns is not one that has had much investigation. Current literature only provides

integration methods which deal mainly with gaps over 1m in length and are, according to [18], not always completely accurate with errors of up to 20%.

- In both cases, the positive and negative impulses recorded higher level of U_{50} voltages when comparing to both the theoretical LPM method as well as the sparkover voltage for gaps less than 1 metre. This can possibly be attributed to a number of factors such as the insulator effecting the distribution of the electric field and therefore influencing the point of breakdown. Pagini et al [18] does not consider the use of insulators in the development of the leader progression model.

- The CFO voltages for a single arcing horn setup corresponded closely to the CFO voltage for the rotated 90° setup despite the dry arcing distance between the both the arcing horn and the end fitting being the same after 60° as illustrated in Figure 4.12. This difference could be attributed to the nature of the surfaces involved and the resulting formation of the avalanche. Thus, the impact of the rotation is not felt after 90°.

- A similarity existed in the results recorded from the leader progression model and the equation from literature for gaps less than 1m. A multiplicative factor was introduced in an attempt to nullify the effect of the insulator in the disturbance of the electric field distribution.

- The insulation co-ordination study illustrated sensitivity of rotation on the value of earth resistance as well as the subsequent theoretical protection of the system under external lightning overvoltage conditions.

- Increased rotation lead to a decrease in the number of backflashovers on a 100km line in a year in the greater Durban area provided the earth resistance remained constant. This was due to an increased lightning current required to cause breakdown in the gap.

- Rotated arcing horns can pose a problem for insulation co-ordination as the CFO for a 90° gap encroaches on the BIL of the transformer. It is therefore necessary to have surge arresters as a source of back up protection.

- Arcing horn rotation does not call for immediate replacement or inspection for that matter. The rotated arrangement allows for a greater system protection by increasing the CFO of the spark gap through its own volt-time curve shift and thereby decreases the BFO rate of the system and the consequential earth faults.

5.1 Recommendations for future work

Future work could include a more detailed simulation perhaps using more than one integration method for comparison in order to fully validate the laboratory results for both polarities of impulse. Repeated experimental procedures could also be used to further validate the results found in this dissertation.

References

[1] E. Kuffel, W. Zaengl, and J. Kuffel, *High Voltage Engineering: Fundamentals*, 2nd ed. Newnes, 2000.

[2] M. Gijben, "The lightning climatology of south africa," March 2012.

[3] D. Filipovic-Grcic, B. Filipovic-Grcic, D. Brezak, I. Uglesic, and A. Tokic, "Leader progression model application for calculation of lightning critical flashover voltage of overhead transmission line insulators," in *Lightning Protection (ICLP), 2012 International Conference on*, Sept 2012, pp. 1–8.

[4] M.Z.A. Ab Kadir , I. Cotton, "Application of the insulator coordination gap models and effect of line design to backflashover studies," in *Electrical Power and Energy Systems 32 , 443449*, 2010.

[5] T. Hara and O. Yamamoto, "Modelling of a transmission tower for lightning-surge analysis," *Generation, Transmission and Distribution, IEE Proceedings-*, vol. 143, no. 3, pp. 283–289, May 1996.

[6] A.Phillips, C. Engelbrecht, *Chapter 4- Insulation for Power Frequency-Dependent, EPRI AC Transmission Line Reference Book - 200 kVInsulation.* EPRI, 2005.

[7] L.Zaffanella, *Chapter 5- Switching Surge Performance, EPRI AC Transmission Line Reference Book - 200 kV Insulation.* EPRI, 2005.

[8] F. Gatta, A. Geri, S. Lauria, M. Maccioni, and F. Palone, "Tower grounding improvement vs. line surge arresters: Comparison of remedial measures for high-bfor subtransmission lines," *Industry Applications, IEEE Transactions on*, vol. PP, no. 99, pp. 1–1, 2015.

[9] H. Motoyama, "Experimental study and analysis of breakdown characteristics of long air gaps with short tail lightning impulse," in *IEEE Transactiors on Power Delivery*, 1996.

[10] A.R. Hileman, *Insulation coordination for power systems.* CRC Press, 1999.

[11] P. S. Maruvada, *Chapter 8 - Corona and Gap Discharge Phenomena, EPRI AC Transmission Line Reference Book - 200 kV and Above.* EPRI, 2005.

[12] IEEE, "Standard for power systems - insulation coordination." *IEEE Std 1313-1993*, pp. i–, 1993.

[13] eThekwini Municipality, *Technical specification for 132kV composite insulators*, eThekwini Municipality Std.

[14] W. Diesendorf, *Insulation Co-ordination in High Voltage Electric Power Systems.* Butterworth and Co Ltd., 1974.

[15] J. W.Chisholm, *Chapter 6- Lightning and grounding, EPRI AC Transmission Line Reference Book - 200 kVInsulation.* EPRI, 2005.

[16] IEC 60060-1, *High-voltage test techniques - Part 1: General definitions and test requirements*, September 2010.

[17] T. Thanasaksiri, "Lightning flashover rates of overhead distribution lines applying volt time curve from testing and ieee std.1410-2004," in *Electrical Engineering/Electronics, Computer, Telecommunications and Information Technology (ECTI-CON), 2011 8th International Conference on*, May 2011, pp. 661–664.

[18] A. Pigini, G. Rizzi, E. Garbagnati, A. Porrino, G. Baldo, and G. Pesavento, "Performance of large air gaps under lightning overvoltages: experimental study and analysis of accuracy predetermination methods," *Power Delivery, IEEE Transactions on*, vol. 4, no. 2, pp. 1379–1392, Apr 1989.

[19] G. Gela, "Sparkover performance and gap factors of air gaps below 1 meter," Electric Power Research Institute, Tech. Rep., 1998.

[20] IEC 60060-2, *High-voltage test techniques - Part 2: Measuring systems*, November 2010.

[21] IEEE Std 4-1995, *IEEE Standard Techniques for High-Voltage Testing.*

[22] J. Van Coller, *Insulation Coordination.* School of Electrical and Information Engineering, University of the Witwatersrand, 2005.

[23] J.A Martinez, F. Castro-Aranda, "Lightning performance analysis of transmission lines using the emtp," in *Power Engineering Society General Meeting, 2003, IEEE*, vol. 1, July 2003, pp. 295–300 Vol. 1.

[24] C.R. Bayliss, B.J. Hardy, "Chapter 9 - insulation co-ordination," in *Transmission and Distribution Electrical Engineering (Fourth Edition)*, fourth edition ed., C. Bayliss and B. Hardy, Eds. Oxford: Newnes, 2012.

[25] T. Shindo, Y. Aoshima, I. Kishizima, and T. Harada, "A study of predischarge current characteristics of long air gaps," *Power Apparatus and Systems, IEEE Transactions on*, vol. PAS-104, no. 11, pp. 3262–3268, Nov 1985.

[26] C.F Wagner, A.R Hileman., "Mechanism of breakdown of laboratory gaps," *Power Apparatus and Systems, Part III. Transactions of the American Institute of Electrical Engineers*, vol. 80, no. 3, pp. 604–618, April 1961.

[27] H. L. Rorden, "Insulation levels governed by lightning arresters," *Electrical Engineering*, vol. 69, no. 5, pp. 438–438, May 1950.

[28] A. Haddad, D. German, R. Waters, and Z. Abdul-Malek, "Co-ordination of spark-gap protection with zinc-oxide surge arresters," *Generation, Transmission and Distribution, IEE Proceedings-*, vol. 148, no. 1, pp. 21–28, Jan 2001.

[29] EPRI, *Chapter 6- Improving the Lightning Performance of Transmission Lines, Overhead Transmission Line Lightning and Grounding Reference Book.* Palo Alto, 2013.

[30] D.N.A.Talib, A.H.A. Bakar,H. Mokhlis, "Parameters affecting lightning backflash over pattern at 132kv double circuit transmission lines," in

Power and Energy (PECon), 2012 IEEE International Conference on, Dec 2012, pp. 808–812.

[31] T. Hayashi, Y. Mizuno, and K. Naito, "Study on transmission-line arresters for tower with high footing resistance," *Power Delivery, IEEE Transactions on*, vol. 23, no. 4, pp. 2456–2460, Oct 2008.

[32] J. Marti, "Accurate modelling of frequency-dependent transmission lines in electromagnetic transient simulations," *Power Apparatus and Systems, IEEE Transactions on*, vol. PAS-101, no. 1, pp. 147–157, Jan 1982.

[33] R. Tarko, W. Nowak, *Chapter10 : Lightning Protection of Substations and the Effects of the Frequency-Dependent Surge.* IGI Global, 2013.

[34] IEEE Working Group 3.4.11, "Modeling of metal oxide surge arresters," *Power Delivery, IEEE Transactions on*, vol. 7, no. 1, pp. 302–309, Jan 1992.

[35] ABB, *Surge Arrester Buyers Guide*, 2014.

[36] IEEE Power & Energy Society, *IEEE Guide for the application of transient recovery voltage for AC high voltage circuit breakers*, 2011.

Appendix

A MATLAB CODE : Leader Progression Model

```
function [flash]=leader_length_variable_gap(voltageA,
    voltageB,voltageC,time)
flash=0;

l_A=0; %leader length initially zero for arcing horn
    distance
l_C=0;
l_B=0;
fprintf('\n');
E= 500;%Critical Air Breakdown
dt = time(2,1)-time(1,1); %time step
v_LA = zeros(size(voltageA));
v_LB = zeros(size(voltageB));
v_LC = zeros(size(voltageC));
llA= zeros(size(voltageA)); %length of leaderA
llC= zeros(size(voltageC)); %length of leaderC
llB= zeros(size(voltageB)); %length of leaderB
%h= 1.030; %132kV INITIAL GAP
%r= 0.405; %132kV arcing horn radii
%h = 0.1535; %22kV initial spacing
%r = 0.2071; %22kV ARCING HORN radii
 h = 0.42 ; %88kV initial gap spacing
 r = 0.35 ; %88 arcing horn radii -  check
    measurements

```

```
23 %degrees = 0:1:180;
24 %s = zeros(1,size(degrees));
25
26 %j= 1; %incremental variable to help store length of
       gap
27 %a = -1;
28 c=0;
29 f =0;
30 e = 0;
31 flashA = 0;
32 flashB = 0;
33 flashC = 0;
34
35 for b=180:-1:0 %changing the gap size from largest to
       smallest
36
37     %(ignored for now)
38     %if flash ==1
39     %fprintf('Distance for flashover occurence is d =
           %.2fm.\n\nThe angle at which it took place is b
           = %d degrees.',d,a)
40          %break
41     %end
42
43 x= h;
44 y = r-r*cosd(b);
45 z = r*sind(b);
46
47 d= sqrt(x^2+y^2+z^2); %setting arcing horn gap
48
49 %(ignore)
50 %s(1,j) = d;
51 %j = j+1 ;
52 %a = a +1;
53
```

```
54 l_A=0; %leader length initially zero for set arcing
       horn distance
55 l_C=0;
56 l_B=0;
57
58 for k= 1:length(time) %check using voltage array
       whether backflashover will occur
59      x_1 = d-l_A; %set distance leader/streamer must
            still progress
60      x_2 = d-l_C;
61      x_3 = d-l_B;
62
63 %x= voltage2(k,1)
64 v_leaderA =10^3*d*(((abs(voltageA(k,1)/1000)./x_1)-E))
       ; %determining vleader velocity using iterative
       process
65 v_leaderC =10^3*d*(((abs(voltageC(k,1)/1000)./x_2)-E))
       ;
66 v_leaderB =10^3*d*(((abs(voltageB(k,1)/1000)./x_3)-E))
       ;
67 %dt=time(k+1)-time(k);
68
69 %v_LA(k,1) = v_leaderA;
70 %v_LB(k,1) = v_leaderB;
71 %v_LC(k,1) = v_leaderC;
72
73 if v_leaderA > 0 % leader cannot progress if critical
       E-Field is not exceeded
74 l_A =l_A+abs(v_leaderA)*dt; %increment leader distance
75
76 if flashA == 0
77 llA(k,1)=l_A;
78 v_LA(k,1) = v_leaderA;%store in an array
79 end
80
81 if l_A > d %when leader bridges the gap
```

```
82      flashA = 1;
83      if c== 0 %find the first point at which
            backflashover is realised on phase A
84      fprintf('Phase A FO occurs at %d degrees and
            voltage %d in a time of %d \n', b, voltageA(k
            ,1),time(k,1))
85      c = 1;
86      end
87  end
88
89  end
90
91
92
93  if v_leaderC > 0 % leader cannot progress if critical
        E-Field is not exceeded
94  l_C =l_C+abs(v_leaderC)*dt;
95
96  if flashC == 0
97  llC(k,1)=l_C;
98  v_LC(k,1) = v_leaderC;
99  end
100
101 if l_C > d
102     flashC = 1;
103     if f== 0
104     fprintf('Phase C FO occurs at %d degrees and
            voltage %d in a time of %d \n', b , voltageC(k
            ,1), time(k,1))
105     f = 1;
106     end
107 end
108 end
109
110 if v_leaderB > 0 % leader cannot progress if critical
        E-Field is not exceeded
```

```
111 l_B =l_B+abs(v_leaderB)*dt;
112
113 if flashB == 0
114 llB(k,1)=l_B;
115 v_LB(k,1) = v_leaderB;
116 end
117
118 if l_B > d
119     flashB = 1;
120     if e== 0
121         e = 1;
122     fprintf('Phase B FO occurs at %d degrees and
            voltage %d in a time of %d \n', b, voltageB (k
            ,1), time (k,1))
123     end
124 end
125 end
126
127     if flashA ==1  || flashB ==1 ||flashC ==1 % check
            whether length of leader exceeds length of
            insulator
128
129     flash=1;
130     end
131
132 end %end voltage loop check
133
134
135 end %end distance loop change
136
137 fprintf('\n');
138 if flash == 0
139    disp(['Insulator flashover has not occured',10])
140 end
141
142 figure(1)
```

```
143 plot(time,v_LA,'r'),title('Velocity of Leader A vs
    time'),xlabel('time(s)'),ylabel('Leader Velocity(m.
    s^(-1))'),grid;
144
145 figure(2)
146 plot(time,v_LB,'r'),title('Velocity of Leader B vs
    time'),xlabel('time(s)'),ylabel('Leader Velocity(m.
    s^(-1))'),grid;
147
148 figure(3)
149 plot(time,v_LC,'r'),title('Velocity of Leader C vs
    time'),xlabel('time(s)'),ylabel('Leader Velocity(m.
    s^(-1))'),grid;
150
151 figure (4)
152 plot(time,llA,'m'),title('Length of Leader A vs time')
    ,xlabel('time(s)'),ylabel('Leader Length(m)'),grid;
     %plotting length of leader vs. time
153
154 figure (5)
155 plot(time,llB,'b'),title('Length of Leader B vs time')
    ,xlabel('time(s)'),ylabel('Leader Length(m)'),grid;
156
157 figure(6)
158 plot(time,llC,'c'),title('Length of Leader C vs time')
    ,xlabel('time(s)'),ylabel('Leader Length(m)'),grid;
```

B Drawings

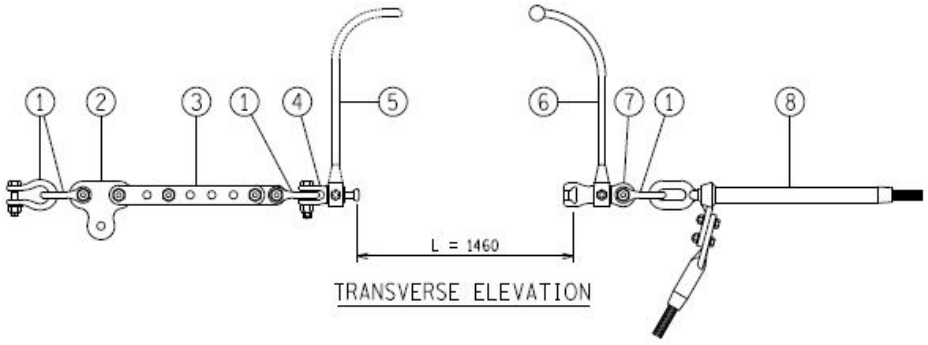

Figure A1: Insulator layout as seen in the eThekwini Municipality drawings

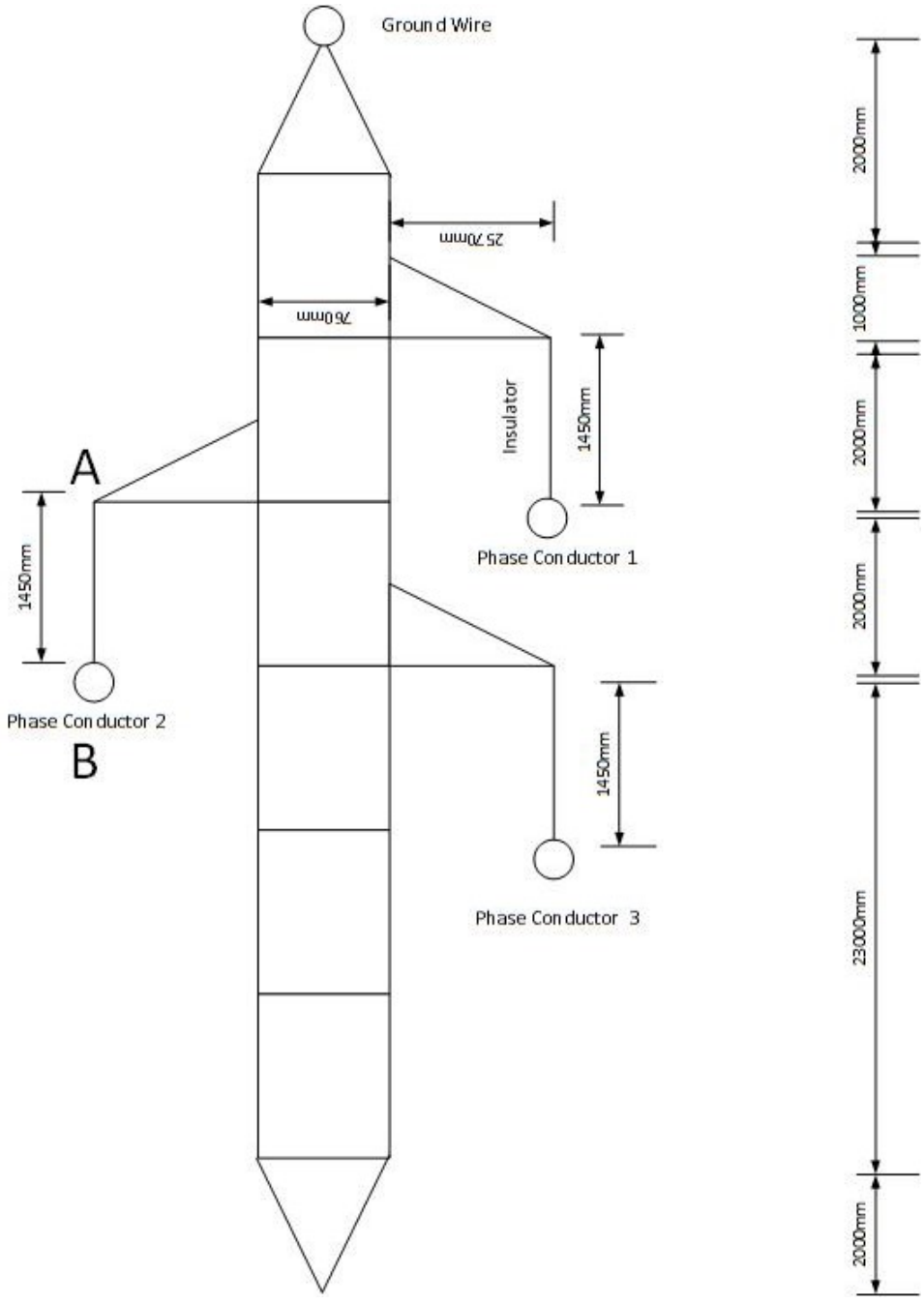

Figure A2: 132kV tower dimensions

C Table of rod-rod gap voltages

Gap spacing (cm)	60 Hz (kV peak)	1.2 × 5 μs) wave (nonstandard)		(1.2 × 50 μs) wave	
		Positive	Negative	Positive	Negative
12	86	115	121	100–107*	116
14	95	134	138	114–125*	132
16	104	153	155	129–142*	147
18	112	170	171	139–153*	158
20	120	188	188	154–161*	176
25	143	234	232	184	217
30	167	277	274	217	249–260*
35	192	320	316	250	283–306*
40	218	362	358	281	313–348*
45	243	405	405	309	347–375*
50	270	445	449	339	382–392*
60	322	525	535	392	455
70	374	605	625	450	525
80	422	690	710	510	585
90	473	765	790	570	670
100	520	845	880	625	715
120	625	990	1040	735	835
140	720	1150	1120	850	965

Figure A3: IEEE 4 standard of rod-rod gap CFO voltages

D Sample Calculations - Surge Arrester

$$L_1 = \frac{15 \times 1.584}{4} = 5.94 \mu H$$

$$R_1 = \frac{65 \times 1.584}{4} = 25.74 \Omega$$

$$L_o = \frac{0.2 \times 1.584}{4} = 0.0792 mH$$

$$R_1 = \frac{100 \times 1.584}{4} = 39.6 \Omega$$

$$C = \frac{100 \times 4}{1.584} = 252.53 pF$$

$$V_{10} = 311 kV \quad for \quad 8/20 \mu s \quad @ \quad 10 kA$$

$$V_{SS} = 272 kV \quad for \quad 30/60 \mu s \quad @ \quad 2 kA$$

E Sample Calculations - N_s

$$N_s = (N_g) \times \frac{28 \times (h)^{0.6} + b}{10} = (5) \times \frac{28 \times (32)^{0.6} + 0}{10} = 112 \quad flashes/100 km/year$$

$$BFO_{rate} = 0.6 \times (112) \times (0.23) = 15.456 \approx 16 \quad flashes/100 km/year$$

F U_{50} testing sample

Up Down Test																					
Voltage Level U	**1**	**2**	**3**	**4**	**5**	**6**	**7**	**8**	**9**	**10**	**11**	**12**	**13**	**14**	**15**	**16**	**17**	**18**	**19**	**20**	**k**	**kU**
																					0	0
																					0	0
																					0	0
44	1		1								1		1		1		1		1		7	308
42		0		1		1		1		0		0		0		0		0		1	10	420
40					0		0		0												3	120
																					0	0
m																				20		
Up																						42

Figure A4: Excel excerpt of an up-down test result

U50	
Parameter	**Value**
Scale Factor	6
Divider Ratio	856
Corrected U50 (kV)	213.5539127

Figure A5: Excel excerpt of U_{50} results